ORIGINAL RESEARCH

# PI3Kα Pathway Inhibition With Doxorubicin Treatment Results in Distinct Biventricular Atrophy and Remodeling With Right Ventricular Dysfunction

Brent A. McLean, PhD; Vaibhav B. Patel, PhD; Pavel Zhabyeyev, PhD; Xueyi Chen, BSc; Ratnadeep Basu, MD, PhD; Faqi Wang, PhD; Saumya Shah, MD; Bart Vanhaesebroeck, PhD; Gavin Y. Oudit, MD, PhD

***Background*—**Cancer therapies inhibiting PI3Kα (phosphoinositide 3-kinase-α)–dependent growth factor signaling, including trastuzumab inhibition of HER2 (Human Epidermal Growth Factor Receptor 2), can cause adverse effects on the heart. Direct inhibition of PI3Kα is now in clinical trials, but the effects of PI3Kα pathway inhibition on heart atrophy, remodeling, and function in the context of cancer therapy are not well understood.

***Method and Results*—**Pharmacological PI3Kα inhibition and heart-specific genetic deletion of p110α, the catalytic subunit of PI3Kα, was characterized in conjunction with anthracycline (doxorubicin) treatment in female murine models. Biventricular changes in heart morphological characteristics and function were analyzed, with molecular characterization of signaling pathways. Both PI3Kα inhibition and anthracycline therapy promoted heart atrophy and a combined effect of distinct right ventricular dilation, dysfunction, and cardiomyocyte remodeling in the absence of pulmonary arterial hypertension. Congruent findings of right ventricular dilation and dysfunction were seen with pharmacological and genetic suppression of PI3Kα signaling when combined with doxorubicin treatment. Increased p38 mitogen-activated protein kinase activation was mechanistically linked to heart atrophy and correlated with right ventricular dysfunction in explanted failing human hearts.

***Conclusions*—**The PI3Kα pathway promotes heart atrophy in mice. The right ventricle is specifically at risk for dilation and dysfunction in the setting of PI3K inhibition in conjunction with chemotherapy. Inhibition of p38 mitogen-activated protein kinase is a proposed therapeutic target to minimize this mode of cardiotoxicity. **(*J Am Heart Assoc*. 2019;8:e010961. DOI: 10.1161/JAHA.118.010961.)**

**Key Words:** anthracycline • heart atrophy • PI3K • remodeling • right ventricle

The PI3K (phosphoinositide 3-kinase) family of lipid kinases is a central transducer of receptor tyrosine kinase signaling and mutations causing unregulated pathway activation among receptor tyrosine kinases; PI3Ks and inhibitory phosphatases, including PTEN (Phosphatase and Tensin Homologue), are among the most commonly occurring sites of mutations in patients with cancer, including gain-of-function mutations in the p110α class 1A catalytic subunit (gene name: *PIK3CA*) in women with breast cancer.[1–3] Cancer therapies can increase the risk of heart disease; anthracycline chemotherapy as well as antibody therapy against HER2 (trastuzumab) and vascular endothelial growth factor pathway inhibitors,[4–11] which may exacerbate traditional cardiovascular risk factors, are often highly represented in patients with cancer. Activation of the PI3Kα pathway, downstream of HER2, is specifically implicated in causing resistance to trastuzumab.[12] PI3K inhibitors may be most effective in cancer therapy in combination with other receptor tyrosine kinase and oncogenic signaling pathway inhibition, as well as cytotoxic chemotherapy agents,[13] inadvertently increasing the chance of adverse, multiple-hit effects on the heart.[14]

Assessment of cardiotoxic cancer therapies in clinical use has focused on left ventricular (LV) remodeling using

*From the Department of Physiology, University of Alberta, Edmonton, Canada (B.A.M., G.Y.O.); Mazankowski Alberta Heart Institute, Edmonton, Canada (B.A.M., V.B.P., P.Z., X.C., R.B., F.W., S.S., G.Y.O.); Division of Cardiology, Department of Medicine, University of Alberta, Edmonton, Alberta, Canada (V.B.P., P.Z., X.C., R.B., F.W., S.S., G.Y.O.); and University College London Cancer Institute, University College, London, England (B.V.).*

Accompanying Data S1, Figures S1 through S4 and Videos S1, S2 are available at https://www.ahajournals.org/doi/suppl/10.1161/JAHA.118.010961

**Correspondence to:** Gavin Y. Oudit, MD, PhD, Division of Cardiology, Department of Medicine, Mazankowski Alberta Heart Institute, University of Alberta, Edmonton, Alberta, Canada T6G 2S2. E-mail: gavin.oudit@ualberta.ca

Received September 19, 2018; accepted April 5, 2019.

## Clinical Perspective

### What Is New?

- Inhibition of PI3Kα (phosphoinositide 3-kinase-α) in female mice causes heart atrophy, and when combined with doxorubicin treatment, it caused right ventricular dilation and dysfunction.
- Combination PI3Kα inhibition and doxorubicin treatment caused activation of p38 mitogen-activated protein kinase, which was implicated in adverse remodeling of the heart.

### What Are the Clinical Implications?

- Use of PI3Kα inhibitors as cancer therapies has the potential to promote heart atrophy, and the right ventricle may be more susceptible to dysfunction and dilation in this setting.
- Assessment of heart morphological characteristics and function in patients receiving PI3Kα inhibitors should capture heart mass as well as biventricular assessment of morphological characteristics and function.
- Inhibition of p38 mitogen-activated protein kinase is a potential target to mitigate heart atrophy and adverse remodeling.

ejection fraction (EF) as an indicator of reduced heart function. However, EF may not capture important remodeling if cancer therapy–related effects do not follow common heart failure pathophysiological characteristics of increased end diastolic volumes, leading to reduced EF. Heart atrophy is common in patients with cancer on the basis of postmortem measurements,[15] and more specifically in cancer cachexia,[16] but the relevance of heart atrophy for heart function has received little attention, as conventional heart failure is commonly characterized by a larger heart mass. However, PI3K signaling is a key mediator of growth factor signaling and regulation of heart mass,[17] which is notable considering the existing propensity for reduced heart mass from cancer.[15] Cancer cachexia is a syndrome of severe loss of body mass, often involving both lean and fat loss, which is a common complication of advanced cancer and cancer therapies, with potential effects on heart mass and function.[18] We recently reported that patients with breast cancer who have received anthracycline and trastuzumab therapy have reduced heart mass as well as biventricular reduction in function compared with healthy controls,[19] consistent with 2 other concurrent reports of reduced heart mass in patients with cancer receiving anthracycline therapy.[20,21] The aim of this study was to determine the effect of PI3Kα inhibition on the cardiac structure and function in female murine models receiving cytotoxic anthracycline (doxorubicin) treatment.

## Methods

The corresponding author will make the data supporting the findings in this study available if a reasonable request is made.

### Animal Use and Drug Treatment Protocols

All animals used were female mice in a C57BL/6 background. Female wild-type mice were treated daily in 5-day cycles with BYL719 (trade name Alpelisib) suspended in corn oil (3.75 mg/mL), or equal volume vehicle, by oral gavage (30 mg BYL719/kg per day), based on dosing previously shown to cause tumor regression by BYL719 in murine models.[22–24] Mice were treated once weekly with doxorubicin dissolved in dimethyl sulfoxide (5% final) and diluted in saline (1.25 mg/mL), or equal volume vehicle, by IP injection (10 mg doxorubicin/kg per week). For MAPK (p38 mitogen-activated protein kinase) inhibition, mice were treated daily in 5-day cycles with SB202190 dissolved in dimethyl sulfoxide (5% final) and diluted in saline (1.25 mg/mL) given by IP injection (5 mg/kg), a dose previously used to limit weight loss in tumor-bearing mice.[25]

Heart-specific genetic deletion of p110α was achieved by breeding mice homozygous for loxP sites (flanked by LoxP; flx) at the p110α gene (*PIK3CA*), as previously described,[26] with Cre recombinase under the control of the αMHC (αMyosin Heavy Chain) promoter (The Jackson Laboratory; Tg[Myh6-cre] 1Jmk/J; No. 009074) back crossed 10 generations. These mice were previously shown to have reduced p110α protein in heart tissue.[27] All experiments were performed in accordance with institutional guidelines, the Canadian Council on Animal Care, and the *Guide for the Care and Use of Laboratory Animals*, published by the US National Institutes of Health (revised 2011). The details on physiological phenotyping, histological and molecular characterization, and statistical analysis used in this study can be found in Data S1.

## Results

### Cotreatment With PI3Kα Inhibitor and Doxorubicin Results in Heart Atrophy and Increased Mortality

To simulate the potential clinical application of cycles of anthracycline with PI3Kα inhibition, wild-type female mice were treated 4 weeks with weekly doses of doxorubicin and 5/week daily doses of the PI3Kα-specific inhibitor, BYL719 (Figure 1A).[27] Phenotyping was performed after 1 to 2 weeks of follow-up to assess persisting effects. Unexpected mortality was observed in the doxorubicin+BYL719 group beginning near the end of the fourth week of treatment and continued

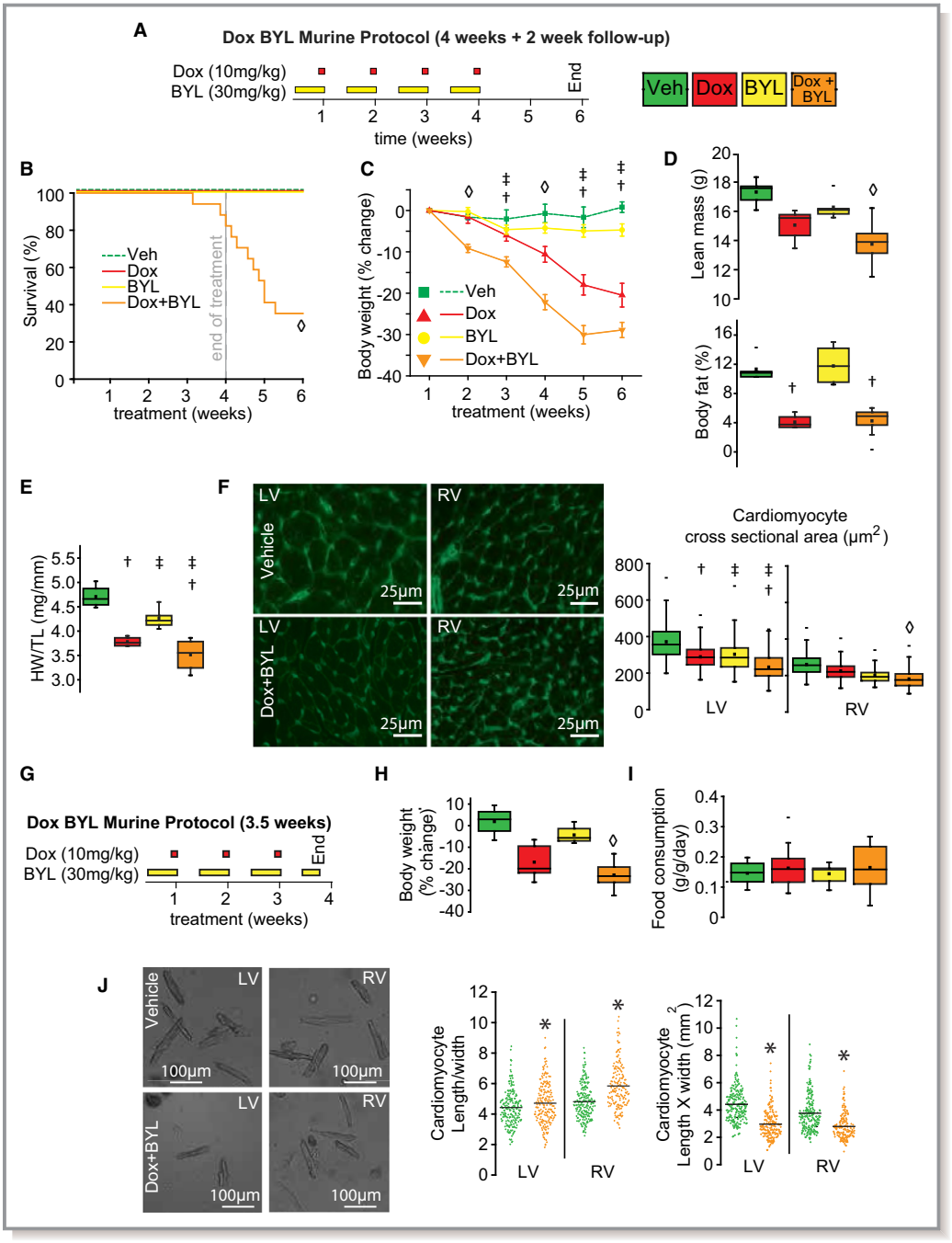


**Figure 1.** Treatment with BYL719 and doxorubicin causes mortality, weight loss, and heart atrophy. **A**, Mice were treated 5 d/wk with daily BYL719 (30 mg/kg) and 1 d/wk with doxorubicin (10 mg/kg), along with single-drug+vehicle groups and a double-vehicle group (Veh), for 4 weeks with a 2-week follow-up period (n=8–17). **B**, Mice treated with doxorubicin+BYL719 had mortality that continued after treatment was stopped. **C**, Doxorubicin and BYL719 caused body weight loss. **D**, Whole body lean mass was reduced by doxorubicin+BYL719, and percentage body fat was reduced by doxorubicin (body composition measured at end of treatment; n=7–12). **E**, Heart weight (HW), normalized to tibial length (TL), was reduced by doxorubicin and BYL719. **F**, Cardiomyocyte cross-sectional area outlined by wheat germ agglutinin staining, measured in both the left ventricle (LV) and right ventricle (RV), was reduced by BYL719 in the RV (n=4). **G**, A 3.5-week treatment protocol caused (**H**) reduced body weight with doxorubicin+BYL719, but (**I**) there was no change in average 24-hour food consumption normalized to body weight. **J**, Doxorubicin+BYL719 treatment caused increased ratio of cardiomyocyte length/width and reduced cardiomyocyte area in the LV and RV (45–82 cells/ventricle from 3 hearts/group). †Doxorubicin effect, ‡BYL719 effect, or ◊doxorubicin+BYL interaction indicates $P \leq 0.05$ in 2-way ANOVA. *$P \leq 0.05$ in unpaired t-test.

over the 2-week follow-up period (Figure 1B). Doxorubicin and BYL719 treatment caused gradual weight loss, which was exacerbated in the doxorubicin+BYL719 group (Figure 1C), whereas body composition analysis showed that doxorubicin caused loss of fat mass and doxorubicin+BYL719 had a combined negative effect on lean mass (Figure 1D). Both doxorubicin and BYL719 caused heart atrophy (Figure 1E), which was consistent with reduction in myocyte cross-sectional area (Figure 1F). These effects occurred in the absence of significant hyperglycemia (Figure S1A), a potential metabolic adverse effect of PI3Kα inhibition.

We next treated an additional cohort for only 3.5 weeks (Figure 1G) for the following reasons: (1) to avoid survival bias in the doxorubicin+BYL719 group, (2) to measure food consumption as a possible confounding cause of weight loss, (3) to collect tissues for molecular investigation under conditions in which direct effects of BYL719 are still present, and (4) to expand our investigation of heart parameters. Although both doxorubicin and BYL719 caused weight loss (Figure 1H), daily measurement of food consumption during the third week of treatment showed stable food consumption normalized to body mass (Figure 1I). Isolation and characterization of right ventricular (RV) and LV cardiomyocytes in a cohort of vehicle- and doxorubicin+BYL719-treated mice confirmed cellular atrophy (reduced area) and eccentric remodeling (increased length/width) with doxorubicin+BYL719, which was more pronounced in the RV (Figure 1J). These results demonstrated a striking increase in mortality and heart atrophy with biventricular cellular remodeling in response to combination doxorubicin+BYL719 therapy.

## Biventricular Remodeling Is Characterized by Reduced Stroke Volume and RV Dilation

We then performed functional cardiac characterization using echocardiography and invasive pressure-volume measurements. Echocardiography showed that doxorubicin treatment caused reduced LV chamber diastolic and systolic dimensions, resulting in decreased LV stroke volume, with a further reduction in response to combination therapy with BYL719 coupled with diastolic dysfunction (Figure 2A and 2B; Table 1) in the absence of pulmonary congestion (Figure S1B). We performed invasive LV pressure-volume analysis to perform load-independent assessment of myocardial contractility, revealing reduced negative maximal rate of contraction and relaxation with doxorubicin treatment (Figure 2C and Table 1). In the 3.5-week treated cohort, distinct LV remodeling was pronounced and characterized by reductions in LV chamber dimensions and stroke volume by BYL719 at this time point (Figure 2D and 2E), suggesting that the effects of BYL719 on LV chamber dimensions may have been partially masked by survival bias, doxorubicin effects, and transience of BYL719 effects in the previous cohort that underwent 4+2 weeks of treatment.

In contrast to reduced volumes seen in the LV, the RVs of doxorubicin+BYL719-treated mice (4+2-week protocol) were dilated, had reduced fractional shortening, and had some irregular septal motion; liver weights were reduced with both treatments, not indicating any hepatic edema (Figure 3A and 3B; Video S1). Pulmonary artery acceleration time (Figure S1B) and the ratio between LV and RV myocyte cross-sectional area (Figure S1C), indicators of pulmonary arterial hypertension, were not significantly altered between experimental groups. Catheterization of the RV was performed 4 to 6 days after the final dose of doxorubicin and 1 to 2 hours after the final dose of BYL719 in 3.5-week treated mice. Relative RV EF was reduced in doxorubicin-treated hearts, with some doxorubicin+BYL719 hearts declining further in relative EF and stroke volume at this early time point. However, there was no alteration in RV filling and peak systolic pressures (Figure 3C and 3D), consistent with the absence of pulmonary arterial hypertension or overt RV failure. Hearts did not show increased apoptosis (terminal deoxynucleotidyl transferase-mediated dUTP nick-end labeling staining) or myocardial fibrosis based on Masson's trichrome and picrosirius red staining in response to doxorubicin+BYL719 (Figure S1F and S1G). Electrocardiographic analysis confirmed intact heart rate, PR interval, and QRS duration, with significant prolongation of the Bazett's correction QT interval, confirming the presence of cardiomyopathy in the absence of conduction disease in the combination treated mice (Figure S2). Specifically, the normal QRS duration and morphological characteristics rule out the presence of bundle branch block. We have performed an in-depth analysis of the electrophysiological effects of PI3Kα inhibition, which demonstrated that the prolonged corrected QT interval is linked to increased late sodium current.[28] We did not observe evidence of overt RV failure in our model, such as elevated RVEDP (right ventricle end diastolic pressure) (Figure 3D), livers were visually normal with reduced weights in treated groups (Figure 3B), and there was no evidence of ascites or hepatic edema. We can only speculate that the RV remodeling and dysfunction we observed could progress to overt RV failure. Our results illustrate a unique cardiotoxicity in doxorubicin+BYL719-treated mice, characterized by RV dilation, decreased LV cardiac output, and myocardial contractility in the absence of pulmonary arterial hypertension or significant cellular death.

## Cardiomyocyte-Specific Loss of PI3Kα Potentiates the Susceptibility to Doxorubicin Toxicity

We next used a female, cardiomyocyte-specific p110α deletion mouse strain (αMHC-Cre) to investigate the direct contribution of the loss of cardiomyocyte p110α function to biventricular

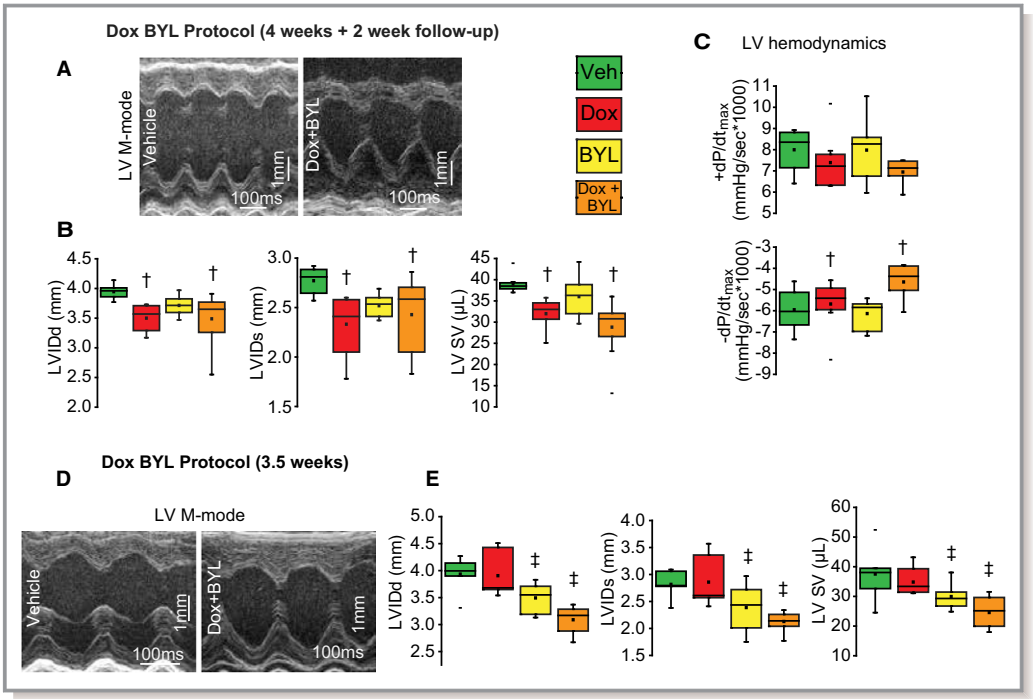


**Figure 2.** Heart function and dimensions in the left ventricle (LV) in response to cardiotoxicity. **A**, LV M-mode images from double treated vehicle- and doxorubicin+BYL719-treated hearts. **B**, LV chamber dimensions (LV internal diameter end diastole [LVIDd] and LV internal diameter end systole [LVIDs]) and LV stroke volume (SV) were reduced by doxorubicin. **C**, LV-positive and LV-negative maximum rates of pressure change ($dP/dt_{max}$) are indicative of impaired contractility. **D**, Example LV M-mode images from double treated vehicle and double-treated doxorubicin+BYL719 hearts at 3.5 weeks of treatment. **E**, Mice treated for 3.5 weeks (n=7–8) have LV chamber dimensions and SV decreased by a BYL719 effect. †Doxorubicin effect, ‡BYL719 effect, or ◇doxorubicin+BYL719 interaction indicates $P \leq 0.05$ in 2-way ANOVA.

remodeling in response to doxorubicin. The αMHC-Cre/p110α cohort of doxorubicin-treated mice did not sustain the high mortality rates seen in the doxorubicin+BYL719 group (4+2-week protocol), so a total of 5 weeks of treatment were completed with 2 weeks of follow-up after the last treatment (5+2-week protocol) (Figure 4A). Doxorubicin treatment caused body weight loss and cardiac atrophy in the αMHC-Cre/p110α mice (Figure 4B). Transthoracic echocardiography showed a dilated RV, reduced fractional shortening with striking interventricular dependence, and a D-shaped septum in the doxorubicin+αMHC-Cre/p110α group (Figure 4C; Table 2; Video S2).

A second cohort was treated for 4 weeks, and invasive RV catheterization was performed, which confirmed RV dilation and reduced relative cardiac output and EF in the αMHC-Cre/p110α+doxorubicin group (Figure 4D and 4E; Table 2). Histological analysis of the lungs demonstrated no overt changes in the pulmonary vasculature or pulmonary fibrosis in doxorubicin+Cre mice and doxorubicin+BYL719 mice (Figure S3). Doxorubicin treatment reduced LV volume and cardiac output coupled with reduced myocardial contractility, as illustrated by the decrease in end-systolic pressure-volume relationship as well as impaired maximal rate of contraction and relaxation (Figure 4F and 4G; Table 2). There was also evidence of diastolic dysfunction in tissue Doppler and isovolumic relaxation time, but not pulse wave Doppler early filling/atrial systole ratio, possibly indicating that load-dependent effects might mask diastolic dysfunction in the pulse wave Doppler early filling/atrial systole ratio parameter.[29]

## Molecular Basis for the Biventricular Cardiomyopathy

We next investigated the molecular pathogenesis of the biventricular myocardial remodeling observed in doxorubicin+Cre/BYL719-treated mice. Consistent with adverse remodeling, expression of heart disease markers showed that doxorubicin increased expression of the β-myosin heavy chain isoform with a trend to increase atrial natriuretic factor in doxorubicin+BYL719-treated hearts (Figure S4A). Phosphorylation and activation of p38 MAPK, which is suppressed by the PI3K/protein kinase B pathway,[30] are linked to the promotion of atrophy and contractile dysfunction.[31] Activation of p38 MAPK was increased by both doxorubicin and BYL719 treatment, resulting in even higher activation by additive effects in doxorubicin+BYL719-treated hearts (Figure 5A). In

**Table 1.** LV Heart Function in Doxorubicin- and BYL719-Treated Mice

| Variable | Vehicle | Doxorubicin | BYL719 | Doxorubicin+BYL719 | *P* Value |
|---|---|---|---|---|---|
| LV echocardiography, n | 8 | 8 | 8 | 12 | . . . |
| LVIDd, mm | 3.9±0.04 | 3.5±0.08 | 3.7±0.06 | 3.5±0.11* | † |
| LVIDs, mm | 2.8±0.05 | 2.3±0.12 | 2.5±0.04 | 2.4±0.11* | † |
| LVFS, % | 30.2±0.6 | 33.7±2.2 | 32.2±0.9 | 30.5±1.6* | NS; *P*=0.085‡ |
| LVEF, % | 58.1±0.9 | 63.1±2.9 | 61.1±1.2 | 58.7±2.3* | NS; *P*=0.098‡ |
| IVRT, ms | 15.4±0.7 | 17.0±0.8 | 15.0±0.3 | 18.2±0.8* | † |
| IVCT, ms | 10.8±0.9 | 12.0±1.0 | 13.8±0.7 | 12.6±1.0* | NS; *P*=0.074§ |
| E/A | 1.7±0.1 | 1.6±0.1 | 1.6±0.1 | 1.7±0.1* | NS |
| E′/A′ | 1.15±0.02 | 1.15±0.06 | 1.11±0.06 | 0.90±0.04* | ‡ |
| LV PV loops, n | 8 | 8 | 8 | 5 | . . . |
| HR, bpm | 439±17 | 407±13 | 430±13 | 400±12* | † |
| ESP, mm Hg | 92.2±1.7 | 90.4±2.8 | 93.1±1.4 | 86.1±1.1* | † |
| EDP, mm Hg | 10.3±1.4 | 5.9±0.9 | 7.4±1.0 | 8.7±0.9* | ‡ |
| $dP/dt_{max}$, mm Hg/s | 7997±348 | 7390±459 | 7979±461 | 6947±298* | NS; *P*=0.079† |
| $-dP/dt_{max}$, mm Hg/s | −5955±333 | −5682±418 | −6134±218 | −4643±416* | † |
| ESV, μL | 9.7±1.6 | 5.5±1.5 | 6.8±0.7 | 5.9±1.2* | NS; *P*=0.079† |
| EDV, μL | 25.4±2.0 | 19.2±1.5 | 25.9±2.5 | 19.6±2.1* | † |
| SV, μL | 18.1±0.7 | 13.7±0.8 | 19.5±2.2 | 13.7±1.6* | † |
| CO, mL/min | 7.7±0.4 | 5.7±0.5 | 8.3±1.0 | 5.4±0.6* | † |
| LVEF, % | 72.4±5.2 | 73.5±5.6 | 74.1±2.7 | 70.2±4.6* | NS |
| ESPVR | 6.5±0.7 | 5.6±0.7 | 7.1±0.7 | 4.2±0.5* | † |
| EDPVR | 0.10±0.02 | 0.16±0.03 | 0.08±0.01 | 0.21±0.05* | † |
| RV PV loops, n | 9 | 7 | 8 | 7 | . . . |
| HR, bpm | 449±26 | 452±35 | 480±18 | 436±25 | NS |
| ESP, mm Hg | 24.9±1.8 | 20.0±1.3 | 19.6±1.6 | 21.7±1.8 | NS |
| EDP, mm Hg | 0.7±0.8 | −0.1±0.9 | 0.1±0.4 | −1.2±1.5 | NS |
| $P_{max}$, mm Hg | 27.0±1.4 | 24.6±0.9 | 23.8±1.9 | 25.9±1.8 | NS |

Values are mean±SEM. A 2-way ANOVA was performed. LV echocardiography was performed on mice treated with doxorubicin and/or BYL719 for 4+1 to 2 weeks of follow-up; LV PV loops were performed at 4+2 weeks of follow-up; RV PV loops were performed at 3.5 weeks of treatment. Bpm indicates beats per minute; CO, cardiac output; $dP/dt_{max}$, maximum rate of positive pressure change; $-dP/dt_{max}$, maximum rate of negative pressure change; E/A, pulse-wave Doppler early filling/atrial systole; E′/A′, tissue Doppler from mitral valve movement from early filling and atrial systole; EDP, end-diastolic pressure; EDPVR, end-diastolic PV relationship; EDV, end-diastolic volume; ESP, end-systolic pressure; ESPVR, end-systolic PV relationship; ESV, end-systolic volume; HR, heart rate; IVCT, isovolumic contraction time; IVRT, isovolumic relaxation time; LV, left ventricular; LVEF, LV ejection fraction; LVFS, LV fractional shortening; LVIDd, LV internal dimension diastolic; LVIDs, LV internal dimension systolic; NS, not significant; $P_{max}$, maximum pressure; PV, pressure-volume; RV, right ventricular; SV, stroke volume.

*Possible survival bias.

†$P \leq 0.05$ for doxorubicin effect.

‡$P \leq 0.05$ for doxorubicin+BYL719.

§$P \leq 0.05$ for BYL719 effect.

the αMHC-Cre/p110α mice, doxorubicin treatment also resulted in a similar pattern of increased p38 activation in the heart (Figure 5B). BYL719, on its own, increased p38 phosphorylation, whereas cardiomyocyte deletion of p110α (Cre) did not, indicating a difference between genetic and pharmacological approaches, possibly because of noncardiomyocyte cells also being affected in the pharmacological model. Activation of p38 is associated with increased oxidation-reduction stress and inflammation[31]; in heart tissue, expression of proinflammatory cytokines (tumor necrosis factor-α and interleukins 6 and 1β) was not upregulated in either the LV or RV with doxorubicin and BYL719 treatment (Figure S1E). However, dihydroethidium fluorescence indicated increased reactive oxygen species production driven by doxorubicin treatment (Figure 5C). To understand the translational aspect of these findings, we next investigated p38 MAPK activation and oxidation-reduction stress in female explanted human hearts with dilated cardiomyopathy, a

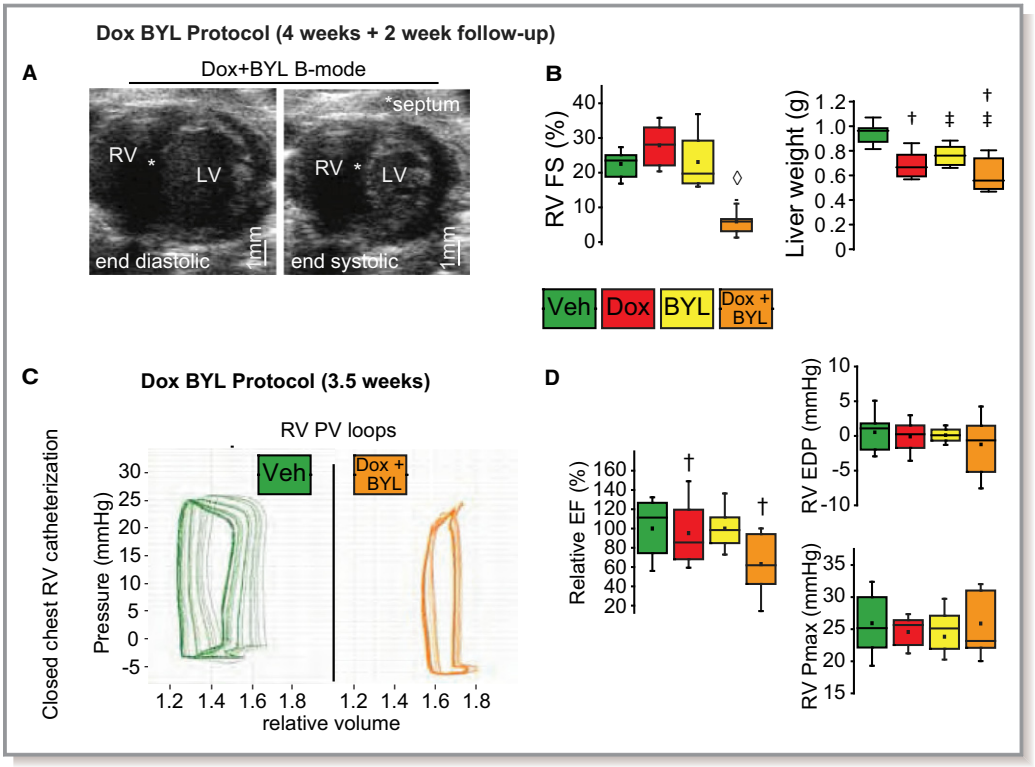


**Figure 3.** Heart function and dimensions in the right ventricle (RV) in response to cardiotoxicity. **A**, Illustrative short-axis B-mode image at end diastole and end systole showing RV dilation and dysfunction in doxorubicin+BYL719-treated hearts. **B**, RV fractional shortening (FS) is reduced by doxorubicin+BYL719, and liver weight is reduced by both doxorubicin and BYL719. **C**, Example of pressure-volume (PV) loops from RV catheterization in mice treated for 3.5 weeks (vehicle only). **D**, Doxorubicin caused a relative reduction in RV ejection fraction (EF) but no increases in end-diastolic pressure (EDP) or maximum pressure ($P_{max}$). LV indicates left ventricle. †Doxorubicin effect, ‡BYL719 effect, or ◇doxorubicin+BYL719 interaction indicates $P \leq 0.05$ in 2-way ANOVA.

disease that involves both ventricles. Interestingly, both p38 activation (Figure 5D) and dihydroethidium fluorescence (Figure 5E) were increased in both ventricles compared with age- and sex-matched controls with a greater mean p38 level in the RV compared with the LV in hearts with dilated cardiomyopathy.

We analyzed FOXO1 (Forkhead Box 01), and SMAD (Mothers Against Decapentaplegic Homolog) 2/3, and atrogin because of their association with muscle atrophy[32]; however, these pathways did not change in a way that would explain our phenotypic observations with doxorubicin+BYL719 treatment. Nuclear localization of FOXO1 was decreased by doxorubicin in the RV, and Smad2/3 was detected only in nonnuclear fractions (Figure S4B). Furthermore, expression of atrogin-1, a regulatory target of FOXO1, was not changed (Figure S4C). We next investigated other potential molecular mechanisms of RV dysfunction. Phosphodiesterase 5 was reported to be increased in the RV in the setting of pulmonary arterial hypertension, and phosphodiesterase 5 inhibition improved RV function.[33] In the present study, phosphodiesterase 5 was increased in doxorubicin-treated LV, with a similar trend in the RV (Figure S4D). We did not proceed to testing the effects of phosphodiesterase 5 inhibition because phosphodiesterase 5 was not particularly elevated in the doxorubicin/BYL719 group, but others have reported heart protection of phosphodiesterase 5 inhibition in doxorubicin-treated mice.[34] Pyruvate dehydrogenase is a metabolic regulator that has also been specifically connected to RV disease.[35] Phosphorylation (inhibitory) was increased in the LV and RV on BYL719 treatment, with no effect of doxorubicin on the LV; but, in the RV, doxorubicin suppressed pyruvate dehydrogenase phosphorylation (Figure S4E). Neither phosphodiesterase 5 nor pyruvate dehydrogenase was specifically altered in doxorubicin+BYL719-treated hearts, and they do not correlate with RV dilation and dysfunction in the manner that we observed with p38 activation.

## Inhibition of p38 Signaling Partially Reversed the Biventricular Cardiomyopathy

Because p38 MAPK inhibitors are currently in clinical trials,[36] we tested a rescue strategy using a p38 MAPK inhibitor in our

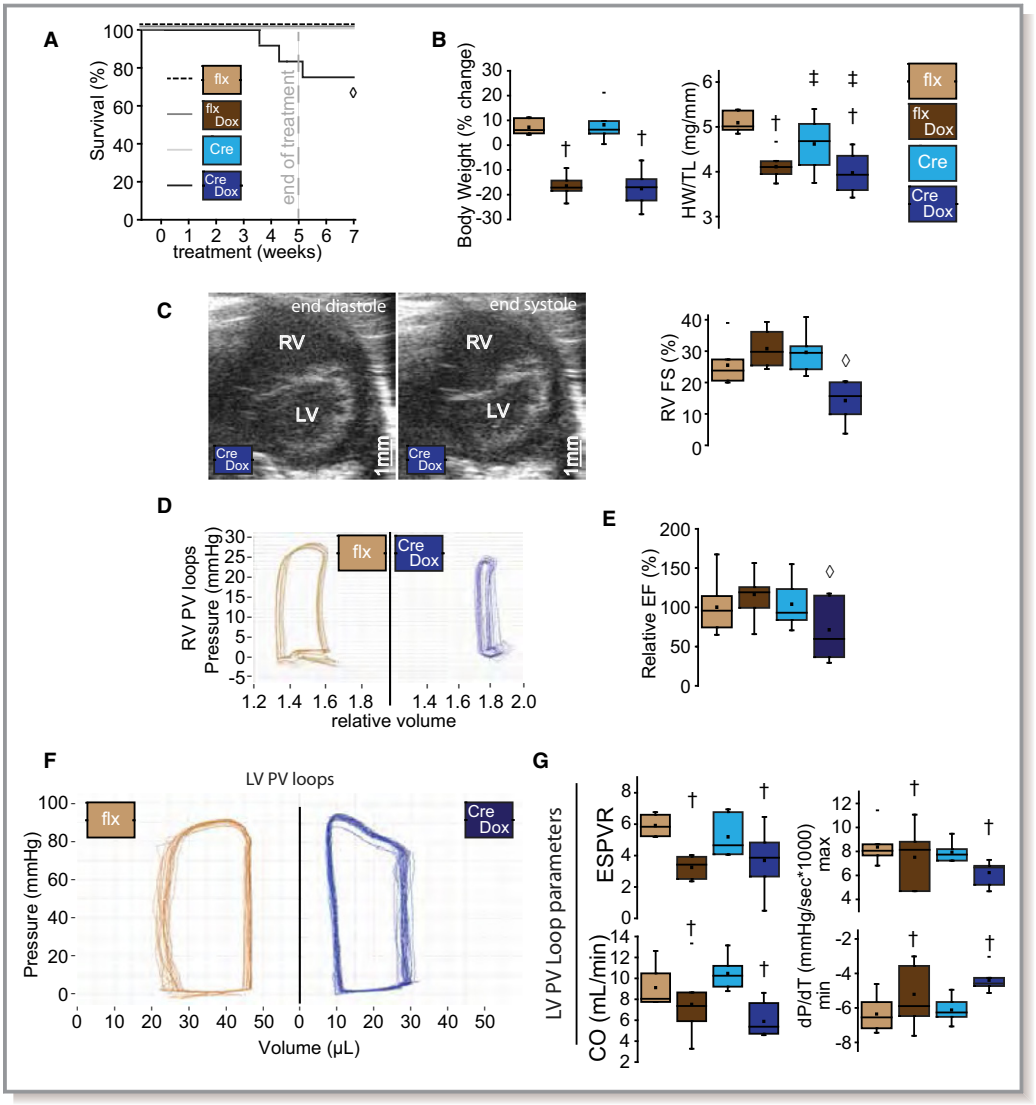


**Figure 4.** Effects of cardiomyocyte-specific deletion of p110α in response to doxorubicin treatment. **A**, Cardiomyocyte-specific deletion of p110α with αMyosin Heavy Chain-Cre recombinase/p110α$^{flx/flx}$ (Cre) or only p110α$^{flx/flx}$ (flx) controls, treated once/week with doxorubicin (10 mg/kg) or vehicle for 5 weeks with a 2-week follow-up period (5+2w); mortality was only seen in doxorubicin-treated Cre mice (n=9–12). **B**, Body weight was reduced by doxorubicin, and heart weight (HW) relative to tibial length (TL) was reduced by doxorubicin and Cre genotype. **C**, Right ventricular fractional shortening (RVFS) was reduced in doxorubicin+Cre; B-mode echocardiographic image shows irregular septal morphological characteristics. **D** and **E**, A second cohort treated for 4 weeks, used for invasive, closed chest catheterization of the RV (RV pressure-volume [PV] loops) had doxorubicin+Cre-dependent reductions in relative RV cardiac ejection fraction (EF) (n=7–9). **F**, Example left ventricular (LV) PV loops for flx vehicle-treated and Cre doxorubicin treated (5+2w). **G**, PV loop analysis: end-systolic pressure-volume relationship (ESPVR), cardiac output (CO), and positive and negative maximum rate of pressure change ($dP/dt_{max}$ and $dP/dt_{min}$, respectively) indicate reduced LV function with doxorubicin treatment. †Doxorubicin effect, ‡genotype effect, or ◊doxorubicin+genotype interaction indicates $P \leq 0.05$ in 2-way ANOVA.

doxorubicin+BYL719 model. Inhibition of p38 MAPK with SB202190 in the doxorubicin+BYL719 group attenuated weight loss and heart atrophy, with a trend toward retaining whole body fat and lean mass (Figure 6A). Cardiomyocyte cross-sectional area was increased in the LV and RV with p38 inhibition (Figure 6B). Invasive pressure-volume analysis of the RV showed reduced ventricular volume associated with increased relative EF and cardiac output (Figure 6C and Table 3) in response to p38 kinase inhibition. The LV stroke volume and fractional shortening increased, which was consistent with improved RV parameters (Figure 6D and Table 3). Dihydroethidium fluorescence, as a marker of

**Table 2.** Heart Function in Doxorubicin-Treated PI3K Cre Mice

| Variable | Flx | Flx Doxorubicin | Cre | Cre Doxorubicin | *P* Value |
|---|---|---|---|---|---|
| LV echocardiography, n | 8 | 7 | 7 | 8 | . . . |
| LVIDd, mm | 3.9±0.04 | 3.6±0.24 | 4.1±0.14 | 3.5±0.33 | * |
| LVIDs, mm | 2.7±0.06 | 2.6±0.23 | 3.0±0.10 | 2.7±0.24 | NS |
| LVFS, % | 30.0±0.7 | 28.3±2.0 | 28.5±0.7 | 24.1±2.8 | NS |
| LVEF, % | 57.9±1.1 | 55.4±3.2 | 55.5±1.1 | 48.0±4.4 | NS; *P*=0.095* |
| IVRT, ms | 15.0±0.5 | 16.8±2.0 | 12.1±0.6 | 19.2±1.5 | * |
| IVCT, ms | 11.2±1.0 | 12.4±1.2 | 10.3±0.3 | 14.2±0.9 | * |
| E/A | 1.5±0.1 | 1.5±0.2 | 1.6±0.2 | 1.7±0.1 | NS |
| E′/A′ | 1.22±0.06 | 0.93±0.07 | 1.24±0.04 | 0.95±0.07 | * |
| LV PV loops, n | 8 | 7 | 6 | 7 | . . . |
| HR, bpm | 439±15 | 406±13 | 439±11 | 341±19 | † |
| ESP, mm Hg | 90.1±3.0 | 87.4±2.6 | 91.1±2.2 | 86.5±3.7 | NS |
| EDP, mm Hg | 7.4±1.1 | 5.9±0.8 | 4.9±0.9 | 6.6±1.2 | NS |
| $dP/dt_{max}$, mm Hg/s | 8359±483 | 7509±868 | 7933±342 | 6231±356.5 | * |
| $-dP/dt_{max}$, mm Hg/s | −6354±357 | −5211±648 | −6121±305 | −4397±250 | * |
| ESV, μL | 12.1 ±3.2 | 12.5 ±3.5 | 10.9 ±2.2 | 7.2 ±1.2 | NS |
| EDV, μL | 34.0±4.9 | 31.1±2.7 | 33.9±2.3 | 24.6±2.4 | NS |
| SV, μL | 22.6±3.2 | 18.6±3.7 | 24.5±2.1 | 17.4±1.5 | * |
| CO, mL/min | 9.9±1.5 | 7.6±1.6 | 10.5±0.6 | 5.9±0.6 | * |
| LVEF, % | 65.1±4.4 | 62.5±10.7 | 69.9±4.8 | 71.6±3.6 | NS |
| ESPVR | 5.9±0.1 | 3.8±0.7 | 4.7±0.5 | 3.7±0.8 | * |
| EDPVR | 0.14±0.03 | 0.13±0.02 | 0.10±0.02 | 0.09±0.03 | NS |
| RV PV loops, n | 8 | 9 | 7 | 7 | . . . |
| HR, bpm | 416±20 | 403±17 | 397±24 | 393±38 | NS |
| ESP, mm Hg | 22.2±1.0 | 23.1±1.5 | 20.7±0.9 | 27.0±3.7 | NS; *P*=0.081* |
| EDP, mm Hg | 0.6±0.3 | 1.2±0.7 | 1.2±0.4 | 2.1±1.2 | NS |
| $P_{max}$, mm Hg | 25.9±0.7 | 25.5±1.4 | 23.2±1.0 | 29.0±3.1 | NS; *P*=0.081† |

Values are mean±SEM. A 2-way ANOVA was performed. Flx denotes LoxP sites inserted flanking the p110 alpha gene. Cre denotes mice with the above flx sites and the addition of Cre recombinase driven by the alpha Myosin Heavy Chain promoter. LV echocardiography was performed on mice treated with doxorubicin for 5+1 to 2 weeks of follow-up; LV (Left ventricle) PV (pressure/volume) loops were performed at 5+2 weeks of follow-up; RV (Right ventricle) PV loops were performed at 4.5 weeks of treatment. Bpm indicates beats per minute; CO, cardiac output; $dP/dt_{max}$, maximum rate of positive pressure change; $-dP/dt_{max}$, maximum rate of negative pressure change; E/A, pulse-wave Doppler early filling/atrial systole; E′/A′, tissue Doppler from mitral valve movement from early filling and atrial systole; EDP, end-diastolic pressure; EDPVR, end-diastolic PV relationship; EDV, end-diastolic volume; ESP, end-systolic pressure; ESPVR, end-systolic PV relationship; ESV, end-systolic volume; HR, heart rate; LVEF, LV ejection fraction; LVFS, LV fractional shortening; LVIDd, LV internal dimension diastolic; LVIDs, LV internal dimension systolic; IVCT, isovolumic contraction time; IVRT, isovolumic relaxation time; NS, not significant; PI3K, phosphoinositide 3-kinase; $P_{max}$, maximum pressure; SV, stroke volume.

*$P \leq 0.05$ for doxorubicin effect.

†$P \leq 0.05$ for Cre+doxorubicin.

oxidation-reduction stress, was not significantly decreased by p38 MAPK inhibition (Figure 6E), consistent with p38 activation being primarily a downstream effect rather than an upstream cause of oxidation-reduction stress. Electrocardiographic analysis showed normalization of the QT interval with p38 inhibition (Figure 6F). These results support a mechanistic role for p38 activation in mediating the adverse doxorubicin+BYL719 effects on the heart and the potential for p38 MAPK inhibition as a therapeutic strategy.

## Discussion

The emergence of targeted cancer therapies contributes to the cumulative risk for heart disease because they are often used in combination with chemotherapeutic agents, such as anthracyclines, and in patients with risk factors for heart disease.[4–9] A striking example of this is the growing list of tyrosine kinase inhibitors indirectly blocking upstream or downstream PI3Kα signaling and direct PI3Kα inhibitors that

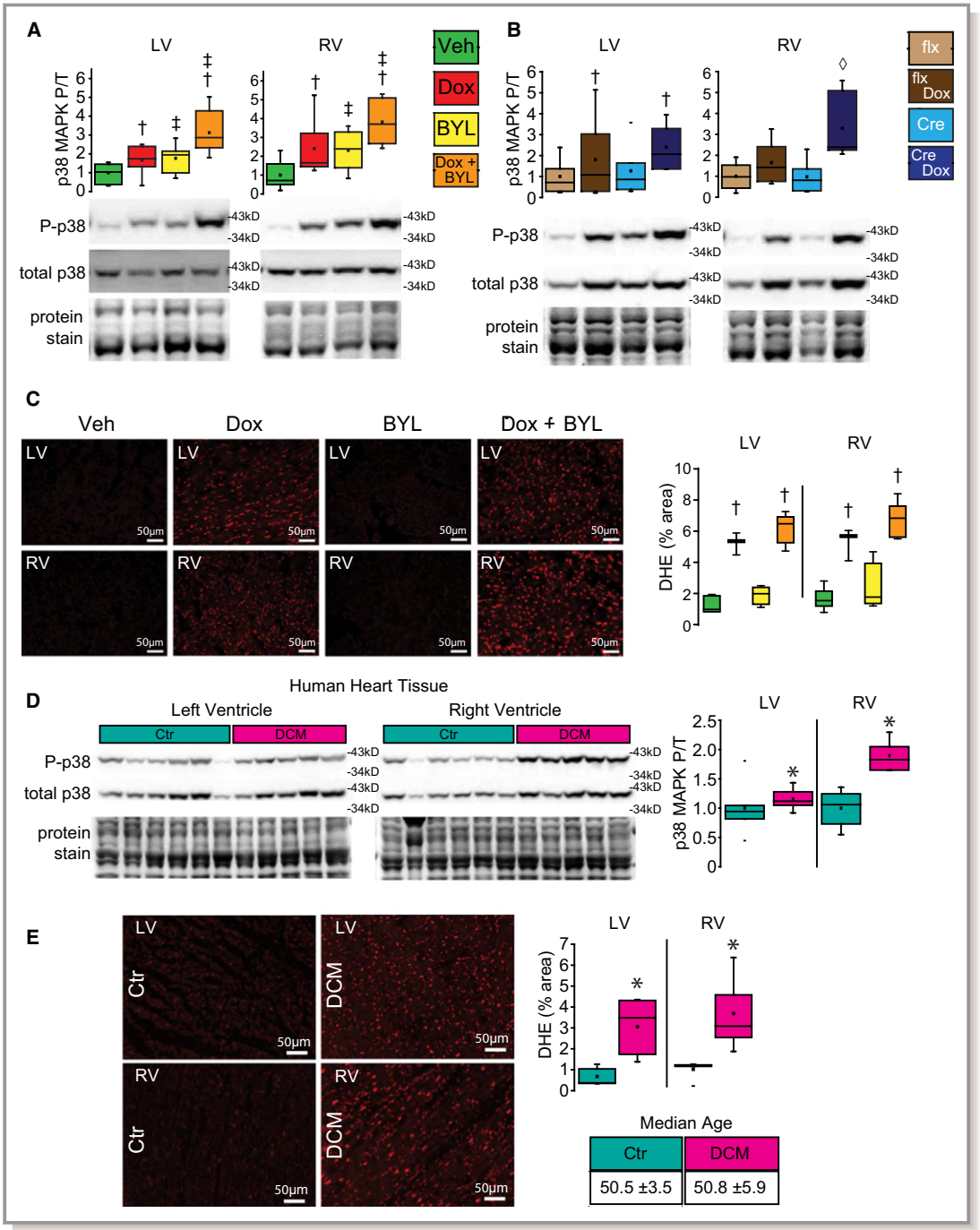


**Figure 5.** Activation of MAPK (p38 mitogen-activated protein kinase) with increased oxidation-reduction stress in diseased murine and human hearts. **A**, Representative Western blots from left ventricular (LV) and right ventricular (RV) heart tissue, 3.5-week protocol, show doxorubicin and BYL719-dependent increases in phosphorylated/total p38 MAPK in both ventricles of wild-type mice (n=6). **B**, Western blot in cardiomyocyte-specific p110α deletion (p110 alpha with LoxP sites only (flx) or also containing alpha Myosin Heavy Chain-Cre recombinase (Cre)) with 4 weeks of doxorubicin treatment showed doxorubicin- and doxorubicin+Cre-related p38 MAPK phosphorylation increases in the LV and RV, respectively (n=6). **C**, Dihydroethidium staining with quantification of dihydroethidium-positive area shows a doxorubicin-dependent increase in oxidative stress (n=3–5). **D**, Female human myocardium from age- and sex-matched nondiseased donor hearts (Ctr; n=6) and nonischemic, extransplanted dilated cardiomyopathy (DCM; n=5) hearts show increased p38 MAPK activation in the LV and RV. **E**, Dihydroethidium staining with quantification of positive area showed increases in DCM hearts compared with age-matched, female Ctr (n=5). *$P \leq 0.05$ in 2-tailed, unpaired *t* test between 2 groups. †Doxorubicin effect, ‡BYL719/genotype effect, or ◊doxorubicin+BYL719/genotype interaction indicates $P \leq 0.05$ in 2-way ANOVA.

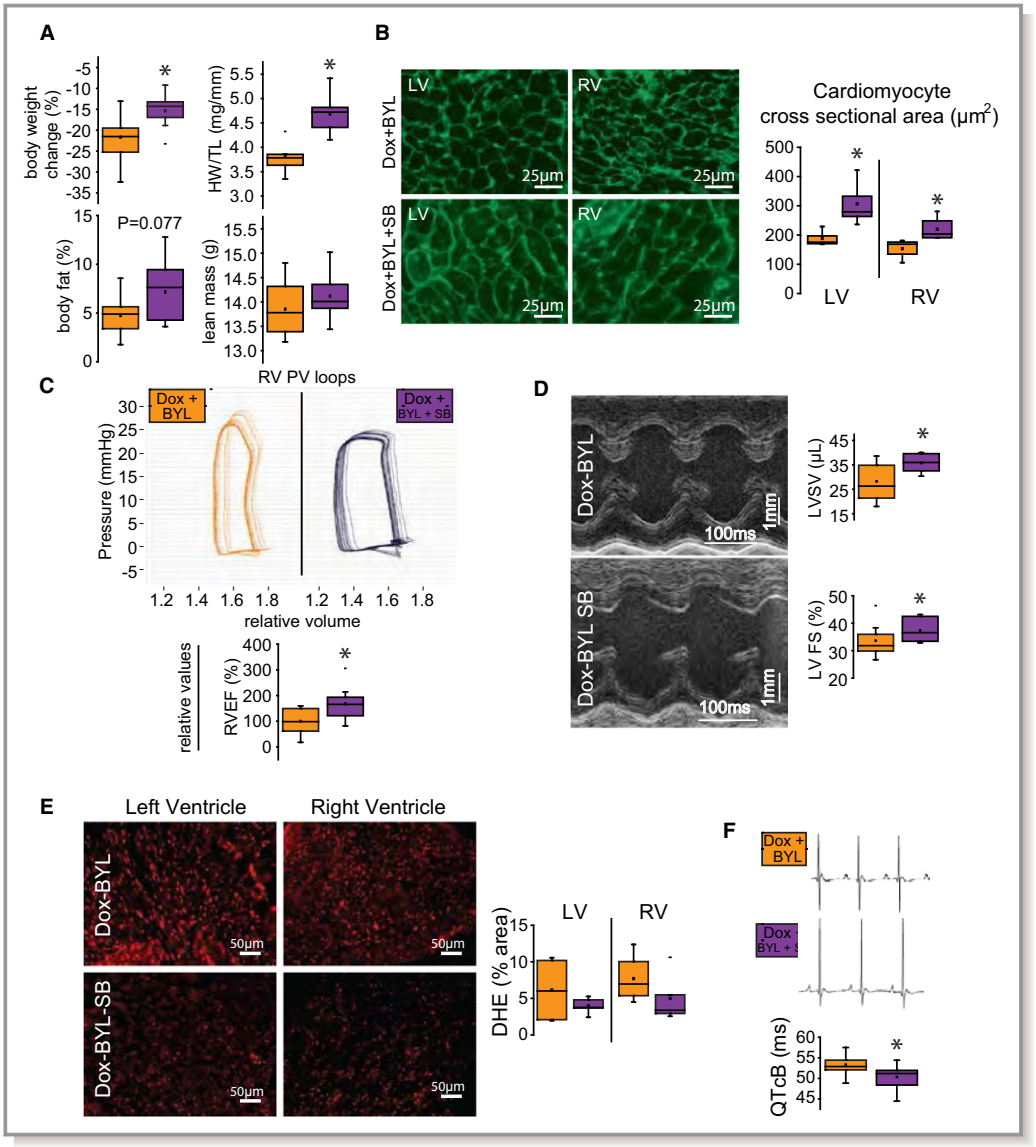


**Figure 6.** Therapeutic inhibition of MAPK (p38 mitogen-activated protein kinase) in doxorubicin- and BYL719-treated mice. Mice were treated with doxorubicin+BYL719 for 3.5 weeks (Figure 1G) but randomized to receive a daily dose (5 d/wk) of the p38 MAPK inhibitor SB202190 (5 mg/kg). **A**, With p38 inhibition, body and heart weight (HW; relative to tibial length [TL]) reduction was attenuated, with trends toward retained body fat and total lean mass (n=9). **B**, Cardiomyocyte cross-sectional area reduction was attenuated with p38 inhibition in the left ventricle (LV) and right ventricle (RV), visualized by wheat germ agglutinin staining (n=5). **C**, Invasive, closed chest catheterization of the RV showed p38 inhibition increased relative RV ejection fraction (RVEF) and relative cardiac output (n=9). **D**, Echocardiography showed an increase in LV stroke volume (LVSV) and fractional shortening (LVFS) with p38 inhibition (n=9). **E**, Dihydroethidium-positive area was not significantly changed by p38 inhibition (n=4–5). **F**, Surface electrocardiographic recordings showed that p38 inhibition reduced QT interval duration (Bazett's correction; QTcB) (n=9). PV indicates pressure-volume. *$P \leq 0.05$ in 2-tailed, unpaired $t$ test.

have the potential to be broadly used in both patients with identified PI3K pathway mutations as well as general adjuvant therapies.[37–39] The compounded cardiovascular risk of PI3Kα inhibitor use in vulnerable groups, such as women with breast cancer, is particularly relevant given the high prevalence of p110α gain-of-function mutations and the large number of clinical trials currently in progress.[40,41] Breast cancer survivors have an increased risk of cardiovascular death compared with a cancer-free comparison cohort,[42] which could be compounded if therapies that increase cancer survival also increase cardiovascular risk when coupled with comorbidities.[43] Preclinical studies can be used to

**Table 3.** LV and RV Echocardiography and Hemodynamics: Doxorubicin+BYL719 With p38 MAPK Inhibition (SB202190)

| Treatment | Doxorubicin+ BYL719 (n=9) | Doxorubicin+ BYL719+ SB202190 (n=9) | *P* Value |
|---|---|---|---|
| LV echocardiography | | | |
| LVIDd, mm | 3.29±0.10 | 3.55±0.05 | * |
| LVIDs, mm | 2.18±0.08 | 2.22±0.07 | NS |
| LVFS, % | 33.7±2.0 | 37.4±1.5 | * |
| LVEF, % | 63.3±2.6 | 68.2±1.9 | * |
| LVSV, μL | 28.2±2.6 | 35.8±1.5 | * |
| RV PV loops | | | |
| HR, bpm | 432.3±19.6 | 458.2±17.6 | NS |
| ESP, mm Hg | 23.3±1.3 | 24.2±0.9 | NS |
| EDP, mm Hg | −0.6±0.9 | 0.9±0.4 | NS |
| $P_{max}$, mm Hg | 26.8±1.2 | 28.2±0.7 | NS |
| SV, % relative | 100±16 | 188±34 | * |
| RVEF, % relative | 100±14 | 168±23 | * |

Values are mean±SEM. Relative values indicated are given with vehicle treated arbitrarily set at 100. LV (Left ventricle) echocardiography was performed; RV (Right ventricle) PV (pressure volume) loops were performed at 3.5 weeks of treatment. Bpm indicates beats per minute; EDP, end-diastolic pressure; ESP, end-systolic pressure; HR, heart rate; LVEF, LV ejection fraction; LVFS, LV fractional shortening; LVIDd, LV internal dimension diastolic; LVIDs, LV internal dimension systolic; LVSV, LV stroke volume; NS, not significant; $P_{max}$, maximum pressure.
*$P \leq 0.05$, independent, 2-tailed *t* test.

understand the type and mechanism of the cardiac risk of PI3Kα inhibition in combination with other perturbations or comorbidities.

We chose to study female animals because of the high prevalence of female patients receiving PI3K pathway inhibitors, including trastuzumab, which acts on the HER2 receptor upstream of PI3K, as well as those in clinical trials for PI3K inhibitors. Sex dimorphic responses in heart remodeling are discussed below, but we have not investigated the different responses to PI3Kα inhibition/deletion in combination with anthracycline therapy in this current study. Using female murine models, we demonstrated that combined doxorubicin and PI3Kα inhibition resulted in increased mortality and a distinct biventricular remodeling (Figure 7), documented by echocardiography and invasive pressure-volume analysis. Biventricular remodeling is best illustrated in the video images of the B-mode echocardiography. RV dilation and reduced fractional shortening with reduced cardiac output are matched to an LV with reduced chamber volumes, likely driven by ventricular interdependence with the potential role of cardiac atrophy. RV dilation and ventricular interdependence also likely lead to impaired LV filling and diastolic dysfunction. Invasive, closed chest measurement of the RV showed normal peak and filling pressures in the presence of PI3Kα inhibition and indicated that pulmonary artery hypertension was not present in our model, consistent with the lack of concentric cardiomyocyte hypertrophy in the RV and normal lung morphological characteristics. We recently reported that deletion or reduction of PI3Kα in cardiomyocytes causes accelerated dilation in a pressure-overload model because of dysregulation of the actin cytoskeletal-severing enzyme gelsolin.[44] We propose that PI3Kα inhibition/deletion may have a similar or even greater detrimental effect in pulmonary hypertension models in which the RV experiences increased afterload.

Rodent models of doxorubicin toxicity often report dilated LV end-diastolic dimensions,[45–47] whereas we observed reduced LV dimensions in our long-term treatment using female mice, possibly because of sex dimorphic responses to these therapies (sex differences were previously reported in response to doxorubicin)[47] or differences in dosage protocols. More important, our findings have been recapitulated by recent clinical studies showing reduced LV mass in response to anthracycline therapy in patients with breast cancer.[20,21] Our chemotherapy regimen also resulted in significant weight loss and reduced heart mass and LV chamber dimensions; heart mass is normally closely correlated with body mass, and anorexia also causes reduced heart mass.[48] We observed weight loss despite normal feeding, indicating a catabolic state not driven by food aversion caused by the treatments. The LV may be partially protected from atrophy because of its higher systolic pressures, which activate prohypertrophy/mass-maintaining signaling in comparison to the RV; consistent with this, in a tumor-driven cachexia model, RV mass was preferentially decreased.[49] In patients with advanced heart failure, cachexia correlated with reduced RV function and worse outcomes compared with patients without cachexia.[50]

Surprisingly, we did not observe significant levels of terminal deoxynucleotidyl transferase-mediated dUTP nick-end labeling staining, fibrosis, or inflammation in doxorubicin- and/or BYL719-treated hearts, indicating that cell death was unlikely to be a significant driver of the biventricular remodeling and dysfunction that we observed. PI3K signaling is a well-known regulator of both cell death and muscle growth; in this study, the dominating phenotype was one of cardiac atrophy, but not cell death. We speculate that drug dose, duration, species, age, and sex could all influence the extent to which doxorubicin and PI3K inhibition have an end effect of cell death and/or muscle atrophy in the heart. Our recent findings (ie, current patients with breast cancer receiving trastuzumab and anthracycline therapy have reduced heart mass and biventricular dysfunction compared with sex- and age-matched controls)[19] support the translational relevance for our findings of heart atrophy in mice receiving doxorubicin and BYL719.

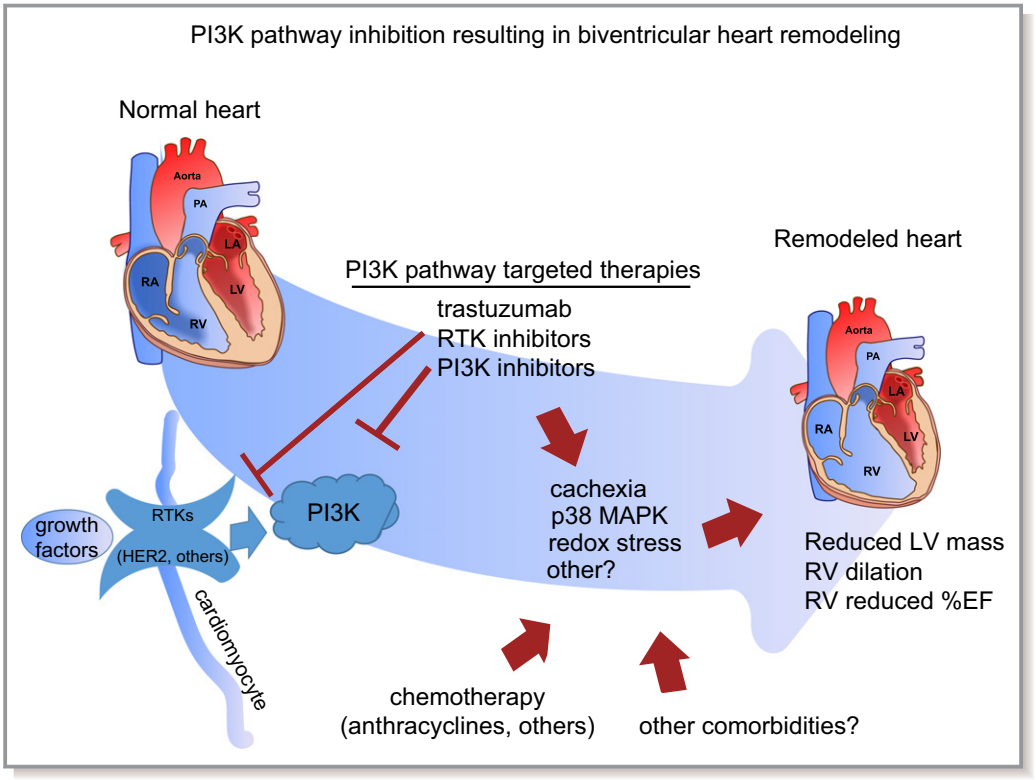


**Figure 7.** Illustration of proposed effects of the phosphoinositide 3-kinase (PI3K) pathway inhibition on the heart in the setting of anthracycline cancer therapy. PI3K pathway inhibition, a central pathway downstream of receptor tyrosine kinases (RTKs), such as HER2 (Human Epidermal Growth Factor Receptor 2), promotes biventricular remodeling with reduced left ventricular (LV) mass and right ventricular (RV) dilation and reduced ejection fraction (EF) in the setting of chemotherapy involving wasting syndrome (cachexia), MAPK (p38 mitogen-activated protein kinase) activation, and oxidation-reduction stress. LA indicates left atrium; MAPK, mitogen-activated protein kinase; PA, pulmonary artery; RA, right atrium.

The pathological processes connected to doxorubicin treatment combined with PI3Kα inhibition we have identified, including oxidative stress indicated by dihydroethidium staining and high levels of p38 MAPK activation, were present similarly in both the LV and RV (Figure 5A and 5C); however, the end morphological changes were distinct between the 2 ventricles. The RV has several inherent differences from the LV, which may contribute to the distinct ventricular remodeling in response to chemotherapy and PI3K inhibition, potentially also in a sex-distinct manner. The RV has reduced defense against oxidation-reduction stress,[51] and molecular changes underpinning ventricular remodeling vary by type and magnitude between the LV and RV.[52,53] Genetic variation in estradiol metabolism and androgen signaling is associated with RV morphological characteristics in a sex-specific manner.[54] RV cardiomyocytes are predominantly longitudinal in orientation, whereas LV myocytes are more radially orientated.[55] Sex differences in RV remodeling are also seen in obese women who exhibit RV remodeling with increased end-diastolic dimension, which is not present in obese men.[56] The clinical relevance of our findings is further strengthened by the observation from the INTERMACS (Interagency Registry for Mechanically Assisted Circulatory Support), in which patients with chemotherapy-related cardiomyopathy receiving Ventricular Assist Devices were predominantly women and more likely to require RV assistance.[57] Indeed, in patients with cancer, female sex is an independent risk factor for cardiac abnormalities after treatment with doxorubicin in association with a greater decrease in LV mass.[58]

We identified that the activation of the p38 MAPK signaling pathway in both the LV and RV may underlie our observed phenotype in female hearts with cardiotoxicity. Doxorubicin can cause p38 activation in cardiomyocytes through negative modulation of the PI3K pathway and promotion of an atrophy gene program,[30] and p38 MAPK activation can have a direct negative inotropic effect at the level of myofilament $Ca^{2+}$ sensitivity.[59] Activation of p38 promotes increased energy expenditure and mitochondrial uncoupling in muscle,[31] and p38 inhibition has beneficial effects in models of muscle atrophy in tumor-bearing cancer cachexia models.[25,60] In female human hearts with dilated cardiomyopathy, we found that both p38 MAPK activation and oxidation-reduction stress

were increased, with greater p38 activation in the RV compared with the LV hearts with dilated cardiomyopathy, possibly indicating an increased propensity for pathological p38 activation in the RV compared with the LV. In patients with cancer and tumor types and therapies that place them at a high risk for cachexia, PI3K inhibition may exacerbate and possibly potentiate pathological weight loss, potentially through increased p38 signaling. Activation of p38 has been linked with skeletal muscle atrophy in cancer cachexia[60] as well as heart dysfunction and remodeling,[61] and p38 MAPK inhibition may be beneficial for both heart[36,61] and cancer treatment.[62] A limitation of our current study is that we used cancer-free mice, so we have not addressed the additional effects that cancers can have on promoting cachexia. Also, the p38 MAPK inhibitor SB202190 has been reported to inhibit other kinases in vitro,[63] so we cannot rule out possible off-target effects contributing to the rescue phenotype we observed. Activation of p38 MAPK signaling is likely only one of many molecular changes contributing to pathological processes with doxorubicin/BYL719 treatment.

We have not assessed the effects of doxorubicin/BYL719 dual treatment on topoisomerase-IIβ, a recognized mediator of doxorubicin-induced damage in the heart.[45] Interestingly, trastuzumab has been reported to cause downregulation of topoisomerase-IIβ in cultured human cardiomyocytes[64]; future studies are needed to determine whether PI3Kα inhibition also has an effect on topoisomerase-IIβ expression or regulation. To our surprise, FOXO1 signaling, which is implicated in skeletal muscle atrophy and regulated by PI3K signaling,[65] was not activated in the heart in this study. We have found previously that assessment of in vivo signaling through the protein kinase B axis downstream of PI3Kα requires close control of the input signals, perhaps the most dominant one being postprandial insulin signaling. In that case, fasting and carefully dosed administration of insulin were required to show that PI3Kα was required for protein kinase B activation.[27] Our current study prioritized heart function assessment with invasive cannulation of the LV or RV as terminal procedures, and we did not control prior feeding. Furthermore, isoflurane anesthesia, which was required for heart cannulation, can also activate the protein kinase B pathway.[66] For these reasons, we believe our current study provides a strong rationale for the relevance of PI3Kα inhibitors for the maintenance of heart mass and morphological characteristics; however, there is much more work to be done to fully understand the signaling cascades downstream of PI3Kα that are responsible for these effects, and we cannot rule out a relevant role for FOXO1.

Our study shows that in female preclinical models, PI3Kα inhibition and doxorubicin resulted in marked RV dilation and dysfunction in the setting of weight loss and heart atrophy. These changes were linked to increased pathological p38 MAPK activation coupled with oxidation-reduction stress. We suspect that weight loss and adverse heart remodeling will be key safety indicators once PI3Kα inhibitors are used for extended periods. PI3Kα inhibition may soon become a mainstay in multidrug combination cancer therapy; a search for "PI3K" on clinicaltrials.gov yielded 472 studies, and "PI3K+cancer" gives 429 studies, most of which use a PI3K inhibitor, often in combination with other therapies. We believe there is a need for a clinical study of heart mass and biventricular morphological characteristics and function in a broad cohort of patients receiving PI3Kα inhibitors. Postmarketing surveillance of patients receiving PI3K inhibitors will also be crucial for assessing the "real-world" effects of these drugs when patients are included who may have been excluded from clinical trials because of compound cardiovascular risks. If PI3K inhibitors do cause heart remodeling in patients with cancer, such as heart atrophy and possible RV dilation, a further question will be to address under what circumstances these effects are reversible on discontinuation of treatment, and at what point these effects are permanent and possibly worsening after discontinuation of treatment. Our current animal study focuses on the PI3Kα isoform, although many PI3K inhibitors target multiple PI3K isoforms that are broadly expressed, creating the potential for additional adverse effects. Our study uses overlapping administration of anthracycline and PI3K inhibitor, but clinical trials of PI3K inhibitors do not currently combine these therapies at the same time; the significance of prior anthracycline therapy versus concurrent anthracycline therapy in combination with PI3K inhibitors for adverse effects on the heart is not clear. Concurrent administration of anthracyclines with mTOR inhibitors has been performed in patients,[67] and similar studies may eventually be performed with PI3K inhibitors. More studies are needed to fully characterize the significance of different PI3K isoform inhibition in combination with other cancer therapies and comorbidities.

## Sources of Funding

McLean is funded by a graduate studentship from Alberta Innovates–Health Solutions (AI-HS). Patel received support from the Heart and Stroke Foundation and AI-HS Postgraduate Fellowships. Oudit is funded by grants from the Canadian Institutes of Health Research, the Heart and Stroke Foundation of Canada, and AI-HS.

## Disclosures

Vanhaesebroeck is an advisory board member and consultant for Karus Therapeutics. The remaining authors have no disclosures to report.

## References


1. Vanhaesebroeck B, Guillermet-Guibert J, Graupera M, Bilanges B. The emerging mechanisms of isoform-specific PI3K signalling. *Nat Rev Mol Cell Biol*. 2010;11:329–341.
2. Lui VW, Hedberg ML, Li H, Vangara BS, Pendleton K, Zeng Y, Lu Y, Zhang Q, Du Y, Gilbert BR, Freilino M, Sauerwein S, Peyser ND, Xiao D, Diergaarde B, Wang L, Chiosea S, Seethala R, Johnson JT, Kim S, Duvvuri U, Ferris RL, Romkes M, Nukui T, Kwok-Shing Ng P, Garraway LA, Hammerman PS, Mills GB, Grandis JR. Frequent mutation of the PI3K pathway in head and neck cancer defines predictive biomarkers. *Cancer Discov*. 2013;3:761–769.
3. She QB, Gruvberger-Saal SK, Maurer M, Chen Y, Jumppanen M, Su T, Dendy M, Lau YK, Memeo L, Horlings HM, van de Vijver MJ, Isola J, Hibshoosh H, Rosen N, Parsons R, Saal LH. Integrated molecular pathway analysis informs a synergistic combination therapy targeting PTEN/PI3K and EGFR pathways for basal-like breast cancer. *BMC Cancer*. 2016;16:587.
4. Romond EH, Perez EA, Bryant J, Suman VJ, Geyer CE Jr, Davidson NE, Tan-Chiu E, Martino S, Paik S, Kaufman PA, Swain SM, Pisansky TM, Fehrenbacher L, Kutteh LA, Vogel VG, Visscher DW, Yothers G, Jenkins RB, Brown AM, Dakhil SR, Mamounas EP, Lingle WL, Klein PM, Ingle JN, Wolmark N. Trastuzumab plus adjuvant chemotherapy for operable HER2-positive breast cancer. *N Engl J Med*. 2005;353:1673–1684.
5. Yeh ET, Tong AT, Lenihan DJ, Yusuf SW, Swafford J, Champion C, Durand JB, Gibbs H, Zafarmand AA, Ewer MS. Cardiovascular complications of cancer therapy: diagnosis, pathogenesis, and management. *Circulation*. 2004;109:3122–3131.
6. Cardinale D, Colombo A, Bacchiani G, Tedeschi I, Meroni CA, Veglia F, Civelli M, Lamantia G, Colombo N, Curigliano G, Fiorentini C, Cipolla CM. Early detection of anthracycline cardiotoxicity and improvement with heart failure therapy. *Circulation*. 2015;131:1981–1988.
7. Ky B, Vejpongsa P, Yeh ET, Force T, Moslehi JJ. Emerging paradigms in cardiomyopathies associated with cancer therapies. *Circ Res*. 2013;113:754–764.
8. Piccart-Gebhart MJ, Procter M, Leyland-Jones B, Goldhirsch A, Untch M, Smith I, Gianni L, Baselga J, Bell R, Jackisch C, Cameron D, Dowsett M, Barrios CH, Steger G, Huang CS, Andersson M, Inbar M, Lichinitser M, Lang I, Nitz U, Iwata H, Thomssen C, Lohrisch C, Suter TM, Ruschoff J, Suto T, Greatorex V, Ward C, Straehle C, McFadden E, Dolci MS, Gelber RD; Herceptin Adjuvant (HERA) Trial Study Team. Trastuzumab after adjuvant chemotherapy in HER2-positive breast cancer. *N Engl J Med*. 2005;353:1659–1672.
9. Bellinger AM, Arteaga CL, Force T, Humphreys BD, Demetri GD, Druker BJ, Moslehi JJ. Cardio-oncology: how new targeted cancer therapies and precision medicine can inform cardiovascular discovery. *Circulation*. 2015;132:2248–2258.
10. Maestrini V, Cheang MH, Kotwinski P, Rosmini S, Lloyd G, Kellman P, Pennell DJ, Montgomery H, Moon JC, Manisty C. Late anthracycline-related cardiotoxicity in low-risk breast cancer patients. *J Am Coll Cardiol*. 2017;69:2573–2575.
11. Chang HM, Moudgil R, Scarabelli T, Okwuosa TM, Yeh ETH. Cardiovascular complications of cancer therapy: best practices in diagnosis, prevention, and management: part 1. *J Am Coll Cardiol*. 2017;70:2536–2551.
12. Berns K, Horlings HM, Hennessy BT, Madiredjo M, Hijmans EM, Beelen K, Linn SC, Gonzalez-Angulo AM, Stemke-Hale K, Hauptmann M, Beijersbergen RL, Mills GB, van de Vijver MJ, Bernards R. A functional genetic approach identifies the PI3K pathway as a major determinant of trastuzumab resistance in breast cancer. *Cancer Cell*. 2007;12:395–402.
13. Fruman DA, Rommel C. PI3K and cancer: lessons, challenges and opportunities. *Nat Rev Drug Discov*. 2014;13:140–156.
14. Jones LW, Haykowsky MJ, Swartz JJ, Douglas PS, Mackey JR. Early breast cancer therapy and cardiovascular injury. *J Am Coll Cardiol*. 2007;50:1435–1441.
15. Kumar NT, Liestol K, Loberg EM, Reims HM, Maehlen J. Postmortem heart weight: relation to body size and effects of cardiovascular disease and cancer. *Cardiovasc Pathol*. 2014;23:5–11.
16. Springer J, Tschirner A, Haghikia A, von Haehling S, Lal H, Grzesiak A, Kaschina E, Palus S, Potsch M, von Websky K, Hocher B, Latouche C, Jaisser F, Morawietz L, Coats AJ, Beadle J, Argiles JM, Thum T, Foldes G, Doehner W, Hilfiker-Kleiner D, Force T, Anker SD. Prevention of liver cancer cachexia-induced cardiac wasting and heart failure. *Eur Heart J*. 2014;35:932–941.
17. Crackower MA, Oudit GY, Kozieradzki I, Sarao R, Sun H, Sasaki T, Hirsch E, Suzuki A, Shioi T, Irie-Sasaki J, Sah R, Cheng HY, Rybin VO, Lembo G, Fratta L, Oliveira-dos-Santos AJ, Benovic JL, Kahn CR, Izumo S, Steinberg SF, Wymann MP, Backx PH, Penninger JM. Regulation of myocardial contractility and cell size by distinct PI3K-PTEN signaling pathways. *Cell*. 2002;110:737–749.
18. Zheng Y, Chen H, Li X, Sun Y. Pay attention to cardiac remodeling in cancer cachexia. *Support Care Cancer*. 2016;24:3253–3259.
19. McLean BA, Hansen R, Paterson DI, White JA, Oudit GY. Breast cancer patients receiving anthracycline chemotherapy and trastuzumab have biventricular dysfunction and reduced heart mass. *J Am Coll Cardiol*. 2018;72:1872–1873.
20. Jordan JH, Castellino SM, Melendez GC, Klepin HD, Ellis LR, Lamar Z, Vasu S, Kitzman DW, Ntim WO, Brubaker PH, Reichek N, D'Agostino RB Jr, Hundley WG. Left ventricular mass change after anthracycline chemotherapy. *Circ Heart Fail*. 2018;11:e004560.
21. Ferreira de Souza T, Quinaglia ACST, Osorio Costa F, Shah R, Neilan TG, Velloso L, Nadruz W, Brenelli F, Sposito AC, Matos-Souza JR, Cendes F, Coelho OR, Jerosch-Herold M, Coelho-Filho OR. Anthracycline therapy is associated with cardiomyocyte atrophy and preclinical manifestations of heart disease. *JACC Cardiovasc Imaging*. 2018;11:1045–1055.
22. Young CD, Pfefferle AD, Owens P, Kuba MG, Rexer BN, Balko JM, Sanchez V, Cheng H, Perou CM, Zhao JJ, Cook RS, Arteaga CL. Conditional loss of ErbB3 delays mammary gland hyperplasia induced by mutant PIK3CA without affecting mammary tumor latency, gene expression, or signaling. *Cancer Res*. 2013;73:4075–4085.
23. Pei Y, Moore CE, Wang J, Tewari AK, Eroshkin A, Cho YJ, Witt H, Korshunov A, Read TA, Sun JL, Schmitt EM, Miller CR, Buckley AF, McLendon RE, Westbrook TF, Northcott PA, Taylor MD, Pfister SM, Febbo PG, Wechsler-Reya RJ. An animal model of MYC-driven medulloblastoma. *Cancer Cell*. 2012;21:155–167.
24. Juvekar A, Hu H, Yadegarynia S, Lyssiotis CA, Ullas S, Lien EC, Bellinger G, Son J, Hok RC, Seth P, Daly MB, Kim B, Scully R, Asara JM, Cantley LC, Wulf GM. Phosphoinositide 3-kinase inhibitors induce DNA damage through nucleoside depletion. *Proc Natl Acad Sci USA*. 2016;113:E4338–E4347.
25. Zhang G, Jin B, Li YP. C/EBPbeta mediates tumour-induced ubiquitin ligase atrogin1/MAFbx upregulation and muscle wasting. *EMBO J*. 2011;30:4323–4335.
26. Graupera M, Guillermet-Guibert J, Foukas LC, Phng LK, Cain RJ, Salpekar A, Pearce W, Meek S, Millan J, Cutillas PR, Smith AJ, Ridley AJ, Ruhrberg C, Gerhardt H, Vanhaesebroeck B. Angiogenesis selectively requires the p110alpha isoform of PI3K to control endothelial cell migration. *Nature*. 2008;453:662–666.
27. McLean BA, Zhabyeyev P, Patel VB, Basu R, Parajuli N, DesAulniers J, Murray AG, Kassiri Z, Vanhaesebroeck B, Oudit GY. PI3Kalpha is essential for the recovery from Cre/tamoxifen cardiotoxicity and in myocardial insulin signalling but is not required for normal myocardial contractility in the adult heart. *Cardiovasc Res*. 2015;105:292–303.
28. Zhabyeyev P, McLean B, Vanhaesebroeck B, Oudit GY. Abstract 15697: acute pharmacological inhibition of PI3Kα by the novel cancer drug, BYL-719, has a pro-arrhythmic effect. *Circulation*. 2018;134:A15697.
29. Nagueh SF, Smiseth OA, Appleton CP, Byrd BF III, Dokainish H, Edvardsen T, Flachskampf FA, Gillebert TC, Klein AL, Lancellotti P, Marino P, Oh JK, Popescu BA, Waggoner AD. Recommendations for the evaluation of left ventricular diastolic function by echocardiography: an update from the American Society of Echocardiography and the European Association of Cardiovascular Imaging. *J Am Soc Echocardiogr*. 2016;29:277–314.
30. Yamamoto Y, Hoshino Y, Ito T, Nariai T, Mohri T, Obana M, Hayata N, Uozumi Y, Maeda M, Fujio Y, Azuma J. Atrogin-1 ubiquitin ligase is upregulated by doxorubicin via p38-MAP kinase in cardiac myocytes. *Cardiovasc Res*. 2008;79:89–96.
31. Puigserver P, Rhee J, Lin J, Wu Z, Yoon JC, Zhang CY, Krauss S, Mootha VK, Lowell BB, Spiegelman BM. Cytokine stimulation of energy expenditure through p38 MAP kinase activation of PPARgamma coactivator-1. *Mol Cell*. 2001;8:971–982.
32. Cohen S, Nathan JA, Goldberg AL. Muscle wasting in disease: molecular mechanisms and promising therapies. *Nat Rev Drug Discov*. 2015;14:58–74.
33. Nagendran J, Archer SL, Soliman D, Gurtu V, Moudgil R, Haromy A, St Aubin C, Webster L, Rebeyka IM, Ross DB, Light PE, Dyck JR, Michelakis ED. Phosphodiesterase type 5 is highly expressed in the hypertrophied human right ventricle, and acute inhibition of phosphodiesterase type 5 improves contractility. *Circulation*. 2007;116:238–248.
34. Nagiub M, Filippone S, Durrant D, Das A, Kukreja RC. Long-acting PDE5 inhibitor tadalafil prevents early doxorubicin-induced left ventricle diastolic dysfunction in juvenile mice: potential role of cytoskeletal proteins. *Can J Physiol Pharmacol*. 2017;95:295–304.
35. Piao L, Fang YH, Cadete VJ, Wietholt C, Urboniene D, Toth PT, Marsboom G, Zhang HJ, Haber I, Rehman J, Lopaschuk GD, Archer SL. The inhibition of pyruvate dehydrogenase kinase improves impaired cardiac function and electrical remodeling in two models of right ventricular hypertrophy: resuscitating the hibernating right ventricle. *J Mol Med (Berl)*. 2010;88:47–60.
36. Muchir A, Wu W, Choi JC, Iwata S, Morrow J, Homma S, Worman HJ. Abnormal p38alpha mitogen-activated protein kinase signaling in dilated cardiomyopathy caused by lamin A/C gene mutation. *Hum Mol Genet*. 2012;21:4325–4333.
37. Wang Q, Liu P, Spangle JM, Von T, Roberts TM, Lin NU, Krop IE, Winer EP, Zhao JJ. PI3K-p110alpha mediates resistance to HER2-targeted therapy in HER2+, PTEN-deficient breast cancers. *Oncogene*. 2016;35:3607–3612.

38. Zhang C, Xu B, Liu P. Addition of the p110alpha inhibitor BYL719 overcomes targeted therapy resistance in cells from Her2-positive-PTEN-loss breast cancer. *Tumour Biol*. 2016;37:14831–14839.
39. McLean BA, Zhabyeyev P, Pituskin E, Paterson I, Haykowsky MJ, Oudit GY. PI3K inhibitors as novel cancer therapies: implications for cardiovascular medicine. *J Card Fail*. 2013;19:268–282.
40. Cancer Genome Atlas Network. Comprehensive molecular portraits of human breast tumours. *Nature*. 2012;490:61–70.
41. Paplomata E, O'Regan R. The PI3K/AKT/mTOR pathway in breast cancer: targets, trials and biomarkers. *Ther Adv Med Oncol*. 2014;6:154–166.
42. Bradshaw PT, Stevens J, Khankari N, Teitelbaum SL, Neugut AI, Gammon MD. Cardiovascular disease mortality among breast cancer survivors. *Epidemiology*. 2016;27:6–13.
43. Groarke JD, Cheng S, Moslehi J. Cancer-drug discovery and cardiovascular surveillance. *N Engl J Med*. 2013;369:1779–1781.
44. Patel VB, Zhabyeyev P, Chen X, Wang F, Paul M, Fan D, McLean BA, Basu R, Zhang P, Shah S, Dawson JF, Pyle WG, Hazra M, Kassiri Z, Hazra S, Vanhaesebroeck B, McCulloch CA, Oudit GY. PI3Kalpha-regulated gelsolin activity is a critical determinant of cardiac cytoskeletal remodeling and heart disease. *Nat Commun*. 2018;9:5390. DOI: 10.1038/s41467-018-07812-8.
45. Zhang S, Liu X, Bawa-Khalfe T, Lu LS, Lyu YL, Liu LF, Yeh ET. Identification of the molecular basis of doxorubicin-induced cardiotoxicity. *Nat Med*. 2012;18:1639–1642.
46. Kim KH, Oudit GY, Backx PH. Erythropoietin protects against doxorubicin-induced cardiomyopathy via a phosphatidylinositol 3-kinase-dependent pathway. *J Pharmacol Exp Ther*. 2008;324:160–169.
47. Moulin M, Piquereau J, Mateo P, Fortin D, Rucker-Martin C, Gressette M, Lefebvre F, Gresikova M, Solgadi A, Veksler V, Garnier A, Ventura-Clapier R. Sexual dimorphism of doxorubicin-mediated cardiotoxicity: potential role of energy metabolism remodeling. *Circ Heart Fail*. 2015;8:98–108.
48. Oflaz S, Yucel B, Oz F, Sahin D, Ozturk N, Yaci O, Polat N, Gurdal A, Cizgici AY, Dursun M, Oflaz H. Assessment of myocardial damage by cardiac MRI in patients with anorexia nervosa. *Int J Eat Disord*. 2013;46:862–866.
49. Borges FH, Marinello PC, Cecchini AL, Blegniski FP, Guarnier FA, Cecchini R. Oxidative and proteolytic profiles of the right and left heart in a model of cancer-induced cardiac cachexia. *Pathophysiology*. 2014;21:257–265.
50. Melenovsky V, Kotrc M, Borlaug BA, Marek T, Kovar J, Malek I, Kautzner J. Relationships between right ventricular function, body composition, and prognosis in advanced heart failure. *J Am Coll Cardiol*. 2013;62:1660–1670.
51. Reddy S, Bernstein D. Molecular mechanisms of right ventricular failure. *Circulation*. 2015;132:1734–1742.
52. Kaufman BD, Desai M, Reddy S, Osorio JC, Chen JM, Mosca RS, Ferrante AW, Mital S. Genomic profiling of left and right ventricular hypertrophy in congenital heart disease. *J Card Fail*. 2008;14:760–767.
53. Rouleau JL, Paradis P, Shenasa H, Juneau C. Faster time to peak tension and velocity of shortening in right versus left ventricular trabeculae and papillary muscles of dogs. *Circ Res*. 1986;59:556–561.
54. Ventetuolo CE, Mitra N, Wan F, Manichaikul A, Barr RG, Johnson C, Bluemke DA, Lima JA, Tandri H, Ouyang P, Kawut SM. Oestradiol metabolism and androgen receptor genotypes are associated with right ventricular function. *Eur Respir J*. 2016;47:553–563.
55. Friedberg MK, Redington AN. Right versus left ventricular failure: differences, similarities, and interactions. *Circulation*. 2014;129:1033–1044.
56. Rider OJ, Lewis AJ, Lewandowski AJ, Ntusi N, Nethononda R, Petersen SE, Francis JM, Pitcher A, Banerjee R, Leeson P, Neubauer S. Obese subjects show sex-specific differences in right ventricular hypertrophy. *Circ Cardiovasc Imaging*. 2015;8:e002454. DOI: 10.1161/CIRCIMAGING.114.002454.
57. Oliveira GH, Dupont M, Naftel D, Myers SL, Yuan Y, Tang WH, Gonzalez-Stawinski G, Young JB, Taylor DO, Starling RC. Increased need for right ventricular support in patients with chemotherapy-induced cardiomyopathy undergoing mechanical circulatory support: outcomes from the INTERMACS Registry (Interagency Registry for Mechanically Assisted Circulatory Support). *J Am Coll Cardiol*. 2014;63:240–248.
58. Lipshultz SE, Lipsitz SR, Mone SM, Goorin AM, Sallan SE, Sanders SP, Orav EJ, Gelber RD, Colan SD. Female sex and drug dose as risk factors for late cardiotoxic effects of doxorubicin therapy for childhood cancer. *N Engl J Med*. 1995;332:1738–1743.
59. Liao P, Wang SQ, Wang S, Zheng M, Zheng M, Zhang SJ, Cheng H, Wang Y, Xiao RP. p38 Mitogen-activated protein kinase mediates a negative inotropic effect in cardiac myocytes. *Circ Res*. 2002;90:190–196.
60. Fukawa T, Yan-Jiang BC, Min-Wen JC, Jun-Hao ET, Huang D, Qian CN, Ong P, Li Z, Chen S, Mak SY, Lim WJ, Kanayama HO, Mohan RE, Wang RR, Lai JH, Chua C, Ong HS, Tan KK, Ho YS, Tan IB, Teh BT, Shyh-Chang N. Excessive fatty acid oxidation induces muscle atrophy in cancer cachexia. *Nat Med*. 2016;22:666–671.
61. Arabacilar P, Marber M. The case for inhibiting p38 mitogen-activated protein kinase in heart failure. *Front Pharmacol*. 2015;6:102.
62. Igea A, Nebreda AR. The stress kinase p38alpha as a target for cancer therapy. *Cancer Res*. 2015;75:3997–4002.
63. Bain J, Plater L, Elliott M, Shpiro N, Hastie CJ, McLauchlan H, Klevernic I, Arthur JS, Alessi DR, Cohen P. The selectivity of protein kinase inhibitors: a further update. *Biochem J*. 2007;408:297–315.
64. Jiang J, Mohan N, Endo Y, Shen Y, Wu WJ. Type IIB DNA topoisomerase is downregulated by trastuzumab and doxorubicin to synergize cardiotoxicity. *Oncotarget*. 2018;9:6095–6108.
65. Glass DJ. PI3 kinase regulation of skeletal muscle hypertrophy and atrophy. *Curr Top Microbiol Immunol*. 2010;346:267–278.
66. Li L, Zuo Z. Isoflurane postconditioning induces neuroprotection via Akt activation and attenuation of increased mitochondrial membrane permeability. *Neuroscience*. 2011;199:44–50.
67. Basho RK, Gilcrease M, Murthy RK, Helgason T, Karp DD, Meric-Bernstam F, Hess KR, Herbrich SM, Valero V, Albarracin C, Litton JK, Chavez-MacGregor M, Ibrahim NK, Murray JL III, Koenig KB, Hong D, Subbiah V, Kurzrock R, Janku F, Moulder SL. Targeting the PI3K/AKT/mTOR pathway for the treatment of mesenchymal triple-negative breast cancer: evidence from a phase 1 trial of mTOR inhibition in combination with liposomal doxorubicin and bevacizumab. *JAMA Oncol*. 2017;3:509–515.

# Supplemental Material

# Data S1.

## Supplemental Methods

***Human Heart Tissue Collection***
Human hearts were collected at the Mazankowski Alberta Heart Institute. Non-failing control (Ctr) hearts were obtained from the Human Organ Procurement and Exchange (HOPE) program, and non-ischemic, dilated cardiomyopathy (DCM) hearts were collected from patients undergoing heart transplant as part of the Human Explanted Heart Program (HELP).[1, 2]

***Echocardiography***
Heart imaging was performed by transthoracic echocardiogram under isoflurane anesthesia (1.5-2%) using Vevo 770 or 3100 with 30MHz transducer (VisualSonics) as previously described.[3] Echocardiography recordings and analysis were performed by an operator blinded to treatment groups and experimental hypothesis.

***Electrocardiogram (ECG)***
Surface electrocardiogram was recorded with mice under light anesthesia (1% inhaled isoflurane) on a heated pad to maintain body temperature using DSI Ponema P3Plus version 5 with measurements recorded in lead I. P and QRS waves were identified by the software, and T waves were manually marked where the wave returned to the isoelectric line.

***Pressure Volume (PV) loops***
Invasive hemodynamic measurements were performed with closed chest under isoflurane anesthesia (1.5-2%) with a 1.2F pressure volume catheter (Transonic Scisense). For left ventricle measurements, the catheter was inserted at the right carotid artery and moved forward, using the pressure trace to determine when the catheter was inside the left ventricle. For right ventricle measurements, the catheter was inserted at the right jugular vein and advanced into the right ventricle, using the pressure trace to indicate when the catheter reached the right ventricle. Due to the irregular chamber shape of the right ventricle, absolute volumes could not be measured, so volumes are compared as relative changes in magnitude. Cannulation recordings and analysis were performed by an operator blinded to treatment groups and experimental hypothesis.

***Body weight, composition and food consumption***
Body weight was measured once per week and drug dosing adjusted. Body composition was measured in live, conscious mice using a NMR-MRI scanner (EchoMRI). Food consumption was estimated by weighing food in a cage at 24hr intervals, with care taken to find any fragments that may have fallen into the bedding. Food consumption was then expressed relative to the total body weight of the animals in that cage (2-3 animals/cage); individual caging of animals was avoided to reduce stress on the animals.

***Blood glucose measurement***
Blood glucose was measured (Bayer monitor and test strips) from a tail vein prick in mice after undergoing an 8 hour daytime fasting period.

***Western blots***

Western blots were performed as follows: tissue was homogenized in CelLytic Lysis Reagent (Sigma) with protease inhibitor cOmplete (Roche), 1 tablet/10mL, and phosphatase inhibitor phosSTOP (Roche), 1 tablet/10mL, using a TissueLyser II (Qiagen). Protein concentrations were standardized using a Bradford assay (Bio-Rad); samples were boiled in a denaturing Laemmli load dye (Bio-Rad) and separated by electrophoresis on a polyacrylamide gel and transferred to a PVDF membrane (Immobilon; Millipore). Membranes were probed using antibodies shown in the following table at 1:1000-1:2000 concentration in Tris buffered saline solution with 1.5% BSA. Samples were loaded with all experimental groups together in a repeating pattern of single biological replicates. For experiments containing 4 groups, a total of 3 biological replicates were loaded onto one 15 well gel and a common inter-gel control sample, made from mixing several samples, was used to normalize quantification and comparison of bands across several gels. All numbers reported are biological replicates.

| **Target Protein** | **Catalogue number** | **Company** |
|---|---|---|
| PDE5a | ab14672 | Abcam |
| P-PDH | AP1062 | EMD Millipore |
| P-p38 | 4511 | Cell Signaling |
| p38 total | 9212 | Cell Signaling |
| FOXO1 | 2880 | Cell Signaling |
| SMAD 2/3 | 5678 | Cell Signaling |
| Histone H3 | 4499 | Cell Signaling |

***Gene Expression***

RNA was extracted by homogenizing (TissueLyser II) frozen tissue samples in TRIzol according to the manufacturer's instructions, and cDNA was synthesized. Gene expression was measured by cDNA quantification using real-time PCR primers and probes (TAQMAN) using a Lightcycler 480 (Roche). Primers (forward and reverse) and probes (all ThermoFisher) are as follows:

| **Protein(*gene*)** | **Type** | **Sequence** |
|---|---|---|
| β- MHC (*Myh7*) | Forward:<br>Reverse:<br>Probe: | 5'-GTGCCA AGG GCC TGA ATG AG-3'<br>5'-GCA AAG GCT CCA GGT CTG A-3'<br>5'-FAM-ATC TTG TGC TAC CCA GCT CTA A-TAMRA-3' |
| ANF (*Nppa*) | Forward:<br>Reverse:<br>Probe: | 5'-GGA GGA GAA GAT GCC GGT AGA-3'<br>5'-GCT TCC TCA GTC TGC TCA CTC A-3'<br>5'-FAM-TGA GGT CAT GCC CCC GCA GG-TAMRA-3' |
| Atrogin-1 (Fbxo32) | | ThermoFisher catalogue # 4331182 |
| TNF-α (*Tnfa*) | Forward:<br>Reverse:<br>Probe: | 5'- ACAAGGCTGCCCCGACTAC-3'<br>5'- TTTCTCCTGGTATGAGATAGCAAATC-3'<br>5'-FAM-TGCTCCTCACCCACACCGTCAGC-TAMRA-3' |
| IL-6 (*Il6*) | Forward:<br>Reverse:<br>Probe: | 5'-ACAACCACGGCCTTCCCTACTT-3'<br>5'-CACGATTTCCCAGAGAACATGTG-3'<br>5'-FAM-TTCACAGAGGATACCACTCCCAACAGACCT-TAMRA-3' |

| | | |
|---|---|---|
| IL-1β (*Il1B*) | Forward:<br>Reverse:<br>Probe: | 5'-AACCTGCTGGTGTGTGACGTTC-3'<br>5'-CAGCACGAGGCTTTTTTGTTGT-3'<br>5'- FAM-TTAGACAGCTGCACTACAGGCTCCGAGATG-TAMRA-3' |

***Subcellular Fractionation***

Fractionation of cell nuclei from heart tissue was performed as previously described.[4] Tissue was homogenized in hypotonic lysis buffer, spun 5min at 100g, then SN spun 10min at 2,000g. The resulting SN was considered the non-nuclear fraction, and the pellet was considered the rough nuclear fraction. The rough nuclear fraction was further purified by ultracentrifugation loaded onto hypotonic lysis buffer + 2.4M sucrose and spun 90min at 100,000g. The pellet was then collected as the final nuclear fraction. The non-nuclear fraction was not further separated into membrane and cytosolic fractions.

***Histological Analysis***

Hearts were arrested in 1M KCl to cause uniform diastole, then fixed in 10% buffered formalin, before paraffin imbedding. Short axis, formalin fixed heart sections were stained with Alexa Fluor 488 conjugated Wheat Germ Agglutinin (WGA) (ThermoFisher) to outline cardiomyocyte cell membranes for cross sectional area measurement.[5] A region of myocardium with cross sectional cardiomyoctes was identified and the area of over 50 cells were measured and averaged to make each single biological replicate shown in the figures.

Terminal deoxynucleotidyltransferase-mediated 2'-deoxyuridine-5'-triphosphate nick-end labeling (TUNEL) staining (Promega) for apoptotic cells was performed according to the manufacturer's instructions. 3-5 randomly chosen regions of the LV and RV were analyzed at 100x magnification from a total of 3 hearts per group. Tissue from a mouse heart that had undergone LAD ligation to cause a myocardial infarction (MI), collected at 1day post-MI, was used as a positive control.[4] Myocardial Fibrosis was visualized by Masson Trichrome staining and Picro Sirius Red staining.[6] Lungs were fixed by cannulation of the trachea and infusing 10% buffered formalin at a height of 10cm; then, a second cannula was inserted into the RV and advanced into the pulmonary artery, tied off, and infused with 10% formalin at a height of 20cm for 20min. Paraffin embedded lung sections were stained with Trichrome. Heart sections frozen in OCT media were stained with dihydroethidium (DHE) as previously described.[7]

Approximately 10 images were randomly selected and the intensity quantified by an operator blinded to experimental groups and the hypothesis of the experiment. The average of these experimental replicates were averaged to determine the value for each individual biological replicate.

***Statistics, graphs and randomization***

Data was graphed using box and whisker plots dividing the data into quartiles with the box representing the first and third quartile and the internal band representing the second quartile (median) (Origin 2016); the mean was indicated by a small square, and whiskers show maximum and minimum values within 1.5 of the interquartile range of the box, and individual values are indicated when greater than 1.5x the interquartile range from the upper or lower limit of the box. Statistical analysis was performed using SPSS (IBM SPSS Statistics for Windows, Version 23.0. Armonk, NY: IBM Corp. Released 2015.).

Comparisons between two-level, single factors, used unpaired, two tailed t-tests. A two-way ANOVA was used for two level, two factor analysis to evaluate the effects of the treatment doxorubicin and BYL-719 or genetic deletion of p110α; when the interaction was not significant, a main effects only model was estimated. Cox regression was used for survival analysis. An *a priori* power calculation was not performed due to the exploratory and novel nature of this study. Animals were randomized at the cage level, with all mice within a cage receiving the same treatment. Animal experiments were performed in cycles with all treatment groups represented and unbiased, random assignment of cages to different treatments. Allocation concealment was not performed and was not practical with the visible difference between doxorubicin and saline.

**Figure S1. Phenotyping of doxorubicin and BYL719 treated mice and hearts.**

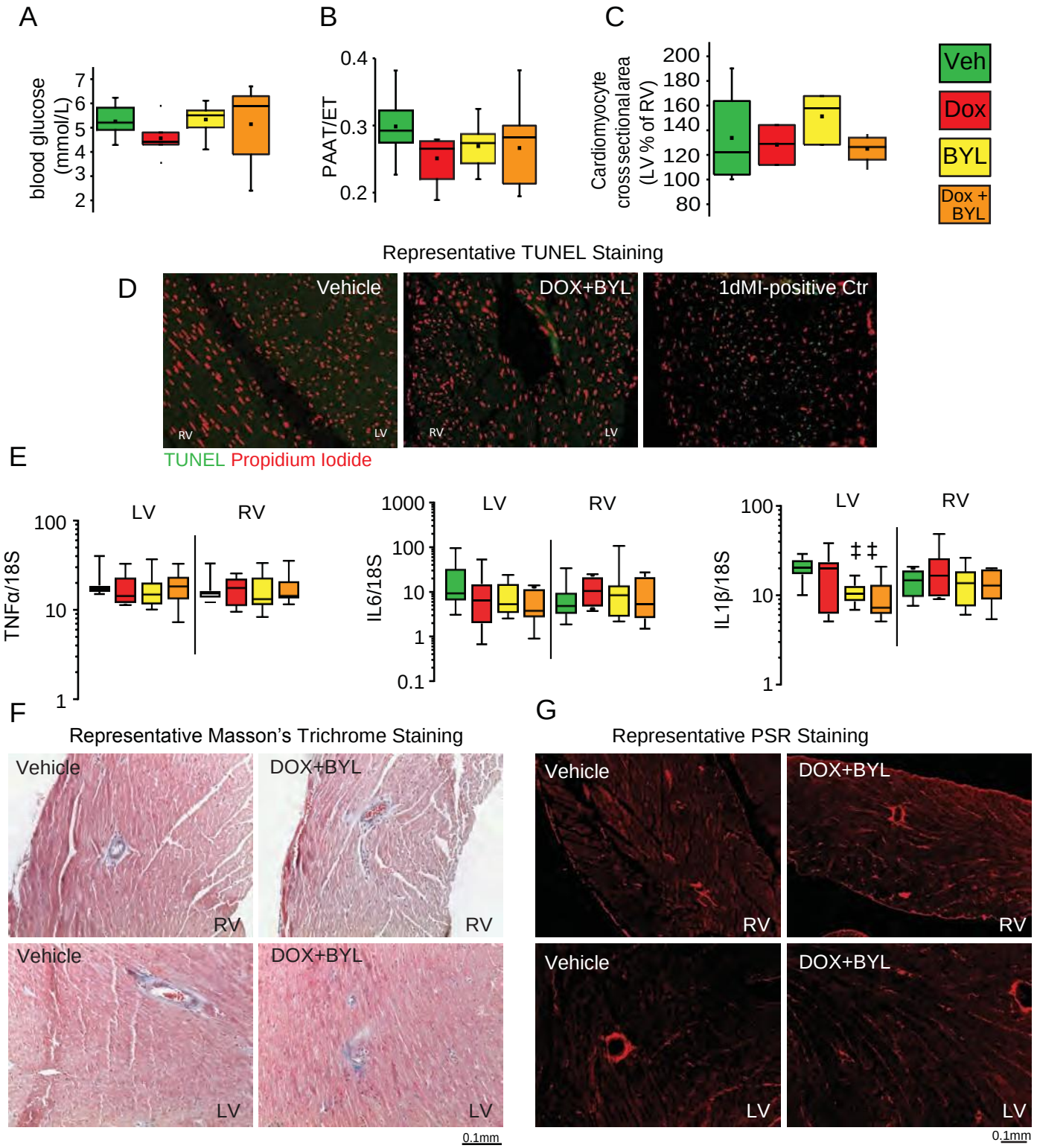


(A) Blood glucose levels after 8hrs fasting (n=4-7). (B) Pulmonary artery acceleration time (PAAT) divided by ejection time (PAAT/ET), measured in pulse wave Doppler echocardiography (n=7-12). (C) Average left ventricle (LV) myocyte cross sectional area is shown as a percentage of right ventricle (RV) myocyte cross sectional area. (D) Terminal deoxynucleotidyltransferase- mediated 2'-deoxyuridine-5'-triphosphate nick-end labeling (TUNEL) and nuclear propidium iodide (PI) (n=3) from 4+2 week treated mice; one day post myocardial infarc- tion (MI) was used as a positive control. (E) Expression of inflammatory markers in LV and RV tissue in 3.5 weeks treated mice (n=7-9). (F) Representative Masson's Trichrome staining and G, PicroSirius Red (PSR) staining of vehicle (Veh) and doxorubicin + BYL719 (Dox+BYL) treated LV and RV sections (n=4) from 4+2 week treated mice. †Dox effect, ‡BYL effect or ◊Dox+BYL interaction indicates P≤0.05 in two-way ANOVA.

**Figure S2. Surface Electrocardiogram.**

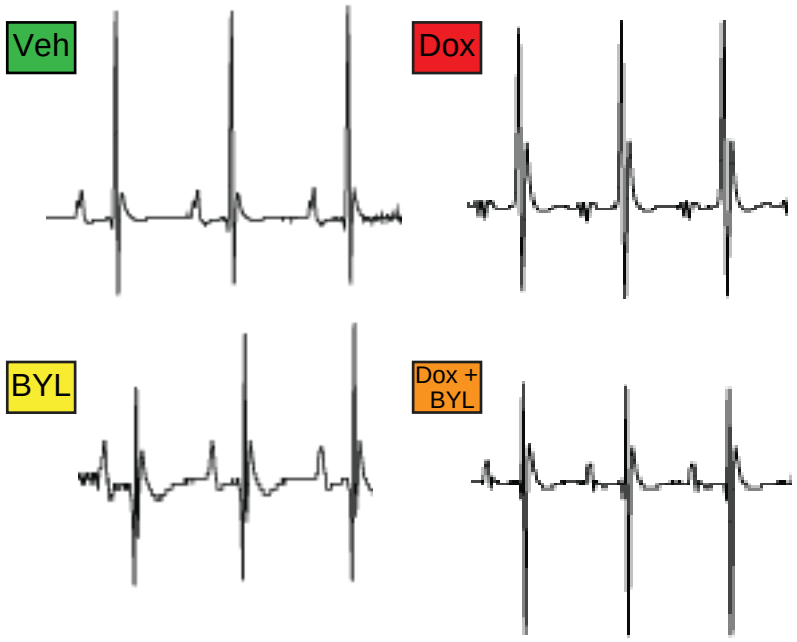


| | Vehicle | Dox | BYL | Dox+BYL | |
|---|---|---|---|---|---|
| n | (9) | (9) | (9) | (8) | |
| HR, bpm | 450 ±22 | 460 ±18 | 439 ±18 | 422 ±13 | ns |
| PR (ms) | 41.3 ±1.4 | 39.7 ±1.2 | 39.9 ±2.1 | 40.6 ±1.4 | ns |
| QRS (ms) | 11.7 ±0.5 | 10.9 ±0.3 | 11.1 ±0.7 | 12.0 ±0.5 | ◊ |
| QT (ms) | 41.3 ±1.4 | 53.8 ±2.6 | 60.7 ±2.8 | 66.2 ±2.9 | ‡ |
| QTcB (ms) | 43.4±1.9 | 47.2 ±2.2 | 51.6 ±1.7 | 55.2 ±1.9 | ‡ |
| QTcF (ms) | 45.7±2.2 | 49.3 ±2.3 | 54.4 ±2.0 | 58.6 ±2.2 | ‡ |

Example electrocardiogram (ECG) traces from WT mice under doxorubicin (Dox) and BYL719 (BYL) or vehicle (Veh) treatment in lead 1; ECG, electrocardiogram; HR, heart rate (recorded at ECG and subsequent pressure/volume (PV) catheter insertion at the end of 3.5 week treatment protocol); ECG derived PR interval, QRS duration and QT interval with QTc (corrected) according to Bazett's (B) and Fridericia's (F) formulas. All values shown are means +/- SEM. †Dox effect, ‡BYL effect or ◊Dox+BYL interaction indicates P≤0.05 in two-way ANOVA.

**Figure S3. Images of formalin fixed lungs stained with trichrome.**

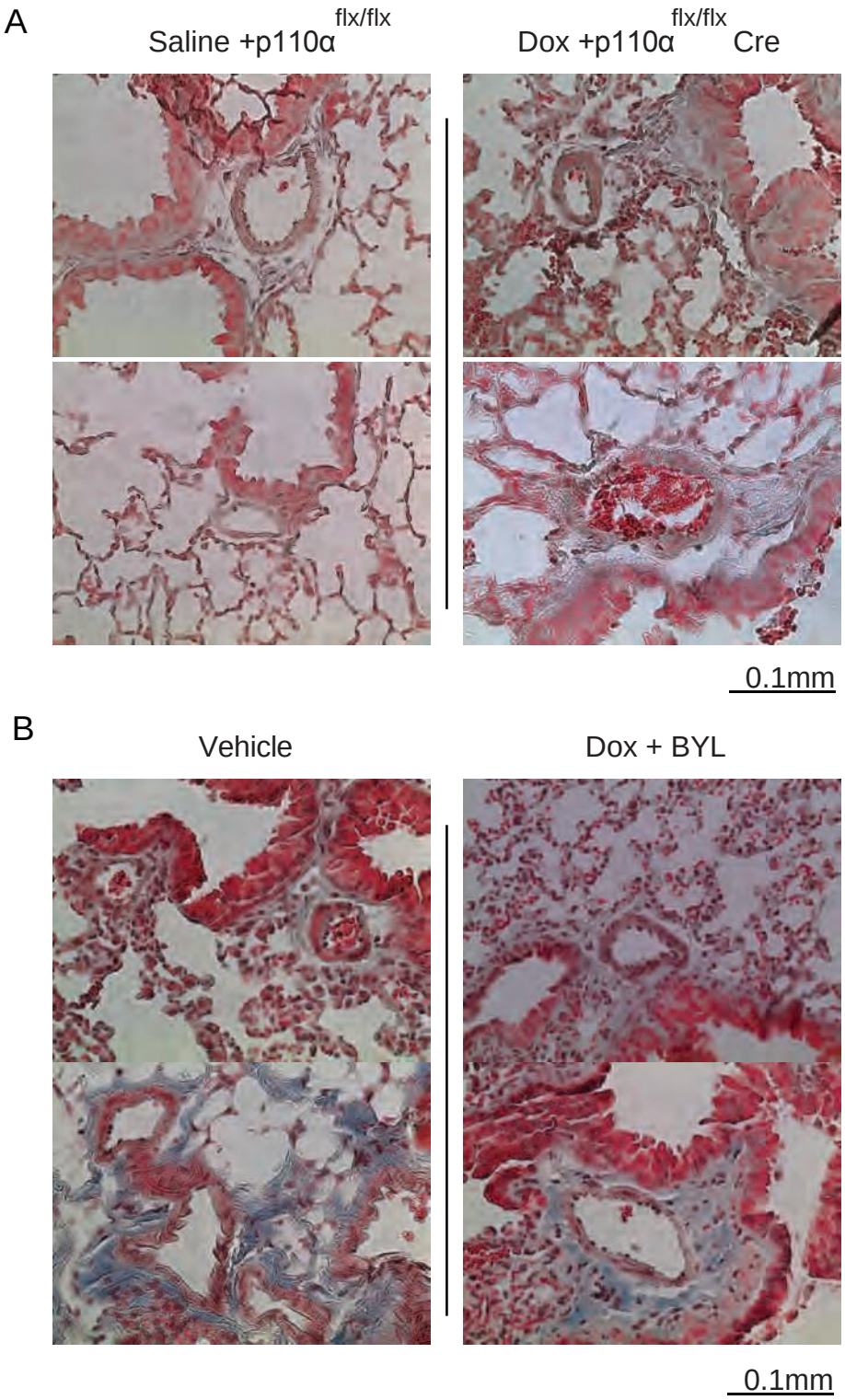


(A) Example images of trichrome stained lungs inflated through cannulation of the trachea and infusion with 10% buffered formalin from no-Dox, p110α flx/flx mice and from 4 weeks Dox treated, p110α flx/flx Cre transgenic mice. (B) Example images of trichrome stained lungs from 3.5 weeks vehicle and Dox+BYL treated mice without lung inflation. Arrows point to artery walls.

**Figure S4. Disease markers and atrophy signaling in doxorubicin and BYL719 treated mice.**

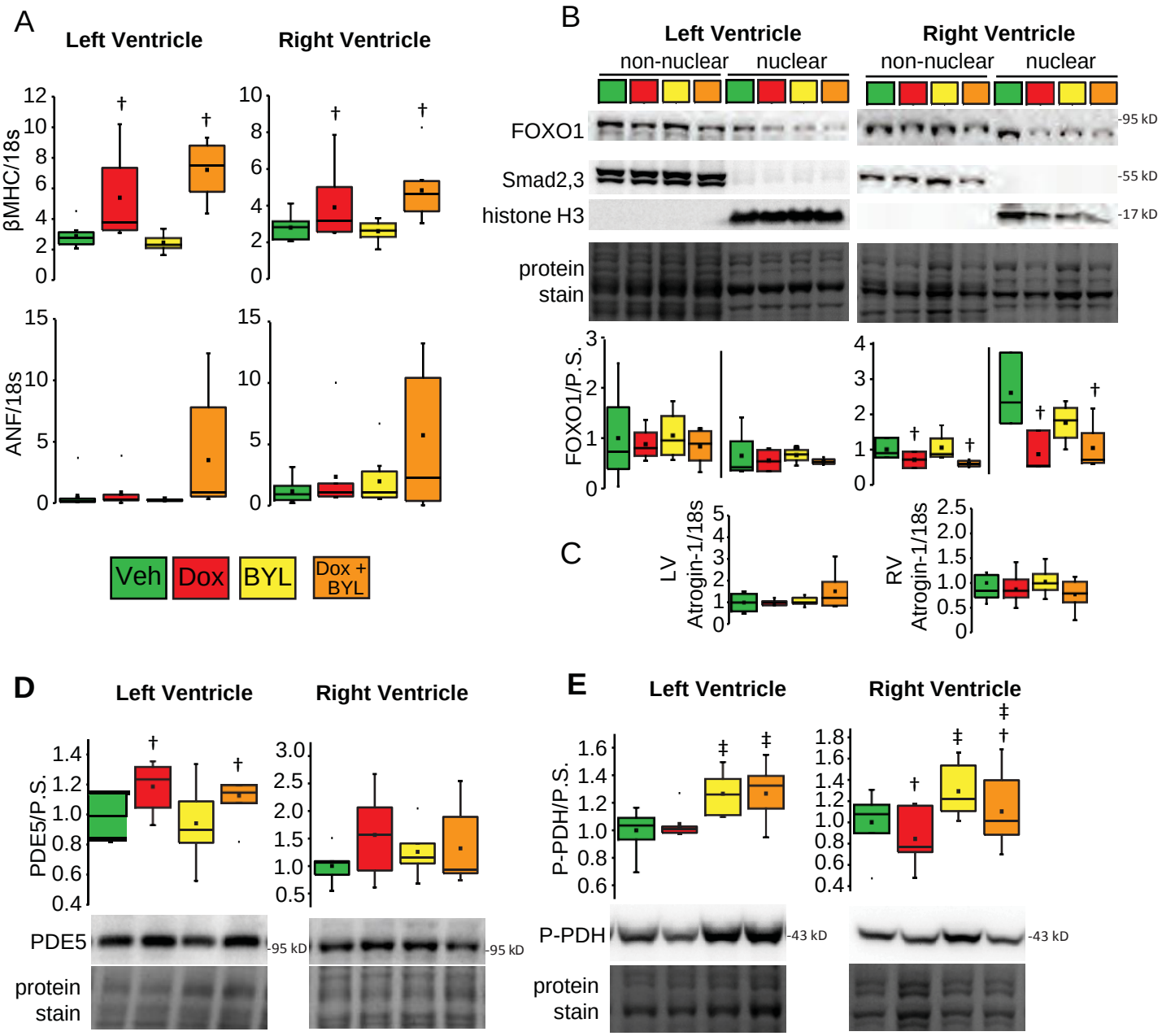


(A) Expression of beta-myosin heavy chain (βMHC) was increased with doxorubicin (Dox) and atrial nature-t ic factor (ANF) was not statistically increased in Dox+BYL719 (BYL) (n=7-9). (B) Representative Western blots and quantification of left ventricle (LV) and right ventricle (RV) heart tissue relative to total protein stain (P.S.) from 3.5 week protocol separated into nuclear and non-nuclear fractions showing decreased nuclear FOXO1 in the RV with Dox treatment; Smad2/3 was only detected in non-nuclear fractions; histone H3 was used as a nuclear marker (n=4-6). (C) Expression of atrogin-1 (Fbxo32) in the LV and RV (n=7-9). (D,E) Western blots in whole LV and RV tissue lysates show a Dox dependent increase in PDE5 in the LV, and a BYL dependent increase in phosphorylated Pyruvate Dehydrogenase (PDH) that is reduced by Dox in the RV (n=6). †Dox effect, ‡BYL effect or ◊Dox+BYL interaction indicates P≤0.05 in two-way ANOVA.

**Supplemental Video Legends:**

**Video S1. Example B-Mode Echocardiography at 4+2 Weeks in Dox/BYL treated mice.** Example video recordings from all treatment groups showing reduced LV chamber volume and RV dilation and dysfunction in Dox+BYL treated group (3 examples shown). Best viewed with Windows Media Player.

**Video S2. Example B-Mode Echocardiography at 5+2 Weeks in Dox treated PI3Kα Cre or Flx only mice.** Example video recordings from all treatment groups showing reduced LV chamber volume and RV dilation and dysfunction in Dox+Cre treated group (2 examples shown). Best viewed with Windows Media Player.

**Supplemental References:**


1. Parajuli N, Valtuille L, Basu R, Famulski KS, Halloran PF, Sergi C and Oudit GY. Determinants of ventricular arrhythmias in human explanted hearts with dilated cardiomyopathy. *European journal of clinical investigation*. 2015;45:1286-96.
2. Patel VB, Mori J, McLean BA, Basu R, Das SK, Ramprasath T, Parajuli N, Penninger JM, Grant MB, Lopaschuk GD and Oudit GY. ACE2 Deficiency Worsens Epicardial Adipose Tissue Inflammation and Cardiac Dysfunction in Response to Diet-Induced Obesity. *Diabetes*. 2016;65:85-95.
3. McLean BA, Zhabyeyev P, Patel VB, Basu R, Parajuli N, DesAulniers J, Murray AG, Kassiri Z, Vanhaesebroeck B and Oudit GY. PI3Kalpha is essential for the recovery from Cre/tamoxifen cardiotoxicity and in myocardial insulin signalling but is not required for normal myocardial contractility in the adult heart. *Cardiovascular research*. 2015;105:292-303.
4. Wang W, McKinnie SM, Patel VB, Haddad G, Wang Z, Zhabyeyev P, Das SK, Basu R, McLean B, Kandalam V, Penninger JM, Kassiri Z, Vederas JC, Murray AG and Oudit GY. Loss of Apelin exacerbates myocardial infarction adverse remodeling and ischemia-reperfusion injury: therapeutic potential of synthetic Apelin analogues. *Journal of the American Heart Association*. 2013;2:e000249.
5. Fan D, Takawale A, Shen M, Wang W, Wang X, Basu R, Oudit GY and Kassiri Z. Cardiomyocyte A Disintegrin And Metalloproteinase 17 (ADAM17) Is Essential in Post-Myocardial Infarction Repair by Regulating Angiogenesis. *Circ Heart Fail*. 2015;8:970-9.
6. Patel VB, Wang Z, Fan D, Zhabyeyev P, Basu R, Das SK, Wang W, Desaulniers J, Holland SM, Kassiri Z and Oudit GY. Loss of p47phox subunit enhances susceptibility to biomechanical stress and heart failure because of dysregulation of cortactin and actin filaments. *Circ Res*. 2013;112:1542-56.
7. Das SK, Wang W, Zhabyeyev P, Basu R, McLean B, Fan D, Parajuli N, DesAulniers J, Patel VB, Hajjar RJ, Dyck JR, Kassiri Z and Oudit GY. Iron-overload injury and cardiomyopathy in acquired and genetic models is attenuated by resveratrol therapy. *Sci Rep*. 2015;5:18132.